Journal of Medicinal Chemistry

pubs.acs.org/jmc

Article

Structure-Based Design of a Chemical Probe Set for the 5-HT$_{5A}$ Serotonin Receptor

Anat Levit Kaplan,[#] Ryan T. Strachan,[#] Joao M. Braz,[#] Veronica Craik, Samuel Slocum, Thomas Mangano, Vanessa Amabo, Henry O'Donnell, Parnian Lak, Allan I. Basbaum,[*] Bryan L. Roth,[*] and Brian K. Shoichet[*]

Cite This: *J. Med. Chem.* 2022, 65, 4201−4217

Read Online

ACCESS | Metrics & More | Article Recommendations | Supporting Information

ABSTRACT: The 5-HT$_{5A}$ receptor (5-HT$_{5A}$R), for which no selective agonists and a few antagonists exist, remains the least understood serotonin receptor. A single commercial antagonist, SB-699551, has been widely used to investigate the 5-HT$_{5A}$R function in neurological disorders, including pain, but this molecule has substantial liabilities as a chemical probe. Accordingly, we sought to develop an internally controlled probe set. Docking over 6 million molecules against a 5-HT$_{5A}$R homology model identified 5 mid-μM ligands, one of which was optimized to **UCSF678**, a 42 nM arrestin-biased partial agonist at the 5-HT$_{5A}$R with a more restricted off-target profile and decreased assay liabilities versus SB-699551. Site-directed mutagenesis supported the docked pose of **UCSF678**. Surprisingly, analogs of **UCSF678** that lost the 5-HT$_{5A}$R activity revealed that 5-HT$_{5A}$R engagement is nonessential for alleviating pain, contrary to studies with less-selective ligands. **UCSF678** and analogs constitute a selective probe set with which to study the function of the 5-HT$_{5A}$R.

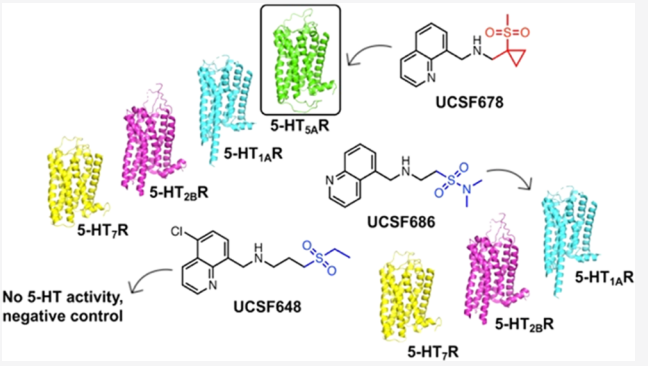

INTRODUCTION

Though G protein-coupled receptors (GPCRs) constitute the largest single family targeted by therapeutic drugs, many remain underexploited.[1−3] Scalable methods to identify small-molecule probes to illuminate their (patho)physiological roles include open-source physical assays,[4] cheminformatic ligand-based virtual screens,[5,6] and structure-based virtual screening campaigns.[7] For these understudied receptors, homology models have been used to template probe discovery, including recent efforts against the orphan receptors GPR68 and GPR65,[8] the primate-exclusive novel opioid receptor MRGPRX2,[9] and others.[10,11]

The human serotonin receptors (5-HTRs) are prototypic drug targets that modulate key neurological processes, including aggression, anxiety, appetite, cognition, learning, memory, mood, sleep, and thermoregulation.[12] Of the 14 serotonin receptor subtypes, the 5-HT$_{5A}$R (HUGO gene name: HTR5A) is perhaps the least understood, largely due to the lack of readily available, selective chemical probes.[13] First cloned in 1994,[14] the human 5-HT$_{5A}$R most closely resembles the 5-HT$_1$R by ligand recognition (e.g., preference for binding methiothepin and ergotamine), Gi/o coupling, and presumed inhibitory autoreceptor function in human cortical and hippocampal pyramidal neurons.[15] 5-HT$_{5A}$Rs are confined primarily to neuronal components of the nervous system, and genetic and pharmacological studies have associated them with several neurological functions (reviewed by Volk and Thomas[13,15]). More recent studies also implicate the 5-HT$_{5A}$R in memory stabilization[16] and memory deficits associated with forgetting and amnesia.[17] Consistent with a 5-HT$_{5A}$R contribution to psychiatric disorders, the upregulation of 5-HT$_{5A}$Rs and activation of a complex Gi signaling cascade are required for the efficacy of selective serotonin reuptake inhibitor (SSRI) antidepressants.[18] Furthermore, dense immunolabeling in the dorsal horn and Onuff's nucleus of the spinal cord suggests that 5-HT$_{5A}$ receptors modulate central motor control, control of pelvic floor musculature, and nociception.[19] Of note, recent in vivo studies demonstrated a 5-HT$_{5A}$R contribution to nociceptive processing in both naïve and injured mice.[20,21]

Notwithstanding its association with these multiple physiological processes, selective probe molecules for the 5-HT$_{5A}$R are unavailable to the community, limiting our ability to test the relevance of these largely genetic associations pharmacologically or to leverage them for therapeutic development.

Received: November 27, 2021
Published: February 23, 2022

https://doi.org/10.1021/acs.jmedchem.1c02031
J. Med. Chem. 2022, 65, 4201−4217

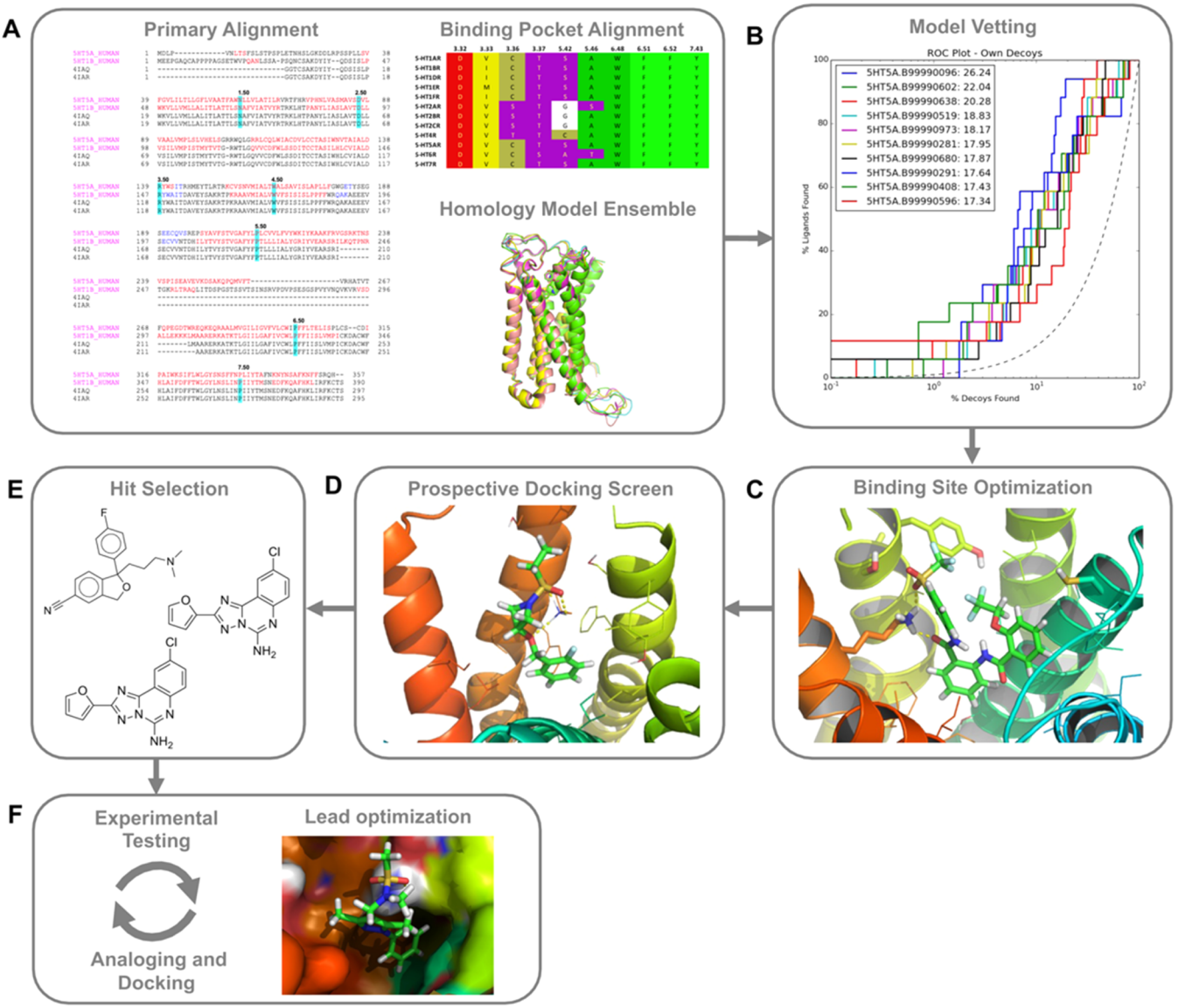

Figure 1. Structure-based strategy for the discovery of novel 5-HT$_{5A}$R chemotypes. (A) Iterative docking and empirical testing begin with the generation of an ensemble of homology models based on the alignment between 5-HT$_{5A}$R and 5-HT$_{1B}$R and relevant crystal structures. Residues highlighted in cyan are the x.50 positions, which are most conserved in each helix. At the top right is the alignment of binding site residues for all 5-HT receptors and their corresponding Ballesteros−Weinstein numbers.[34] At the bottom panel, an ensemble of 1000 homology models was built using MODELER-9v15, with ergotamine retained in the modeling for a ligand-competent orthosteric site. (B) The homology models were then evaluated for their ability to enrich known 5-HT$_{5A}$R ligands over property-matched decoys through docking to the orthosteric site, using DOCK3.7.[35] The enrichment curves for the top 10 performing 5-HT$_{5A}$R models are shown. (C) The binding site of the best-performing model was further optimized through energy minimization. The performance of the minimized model was assessed by redocking the known ligands and decoy molecules and recalculating enrichment factors. (D) Over 6 million "lead-like" molecules from ZINC15 were prospectively screened against the 5-HT$_{5A}$R model by molecular docking. (E) The top 3000 scoring molecules were filtered for chemical novelty against ∼28 000 annotated aminergic ligands (Tc < 0.40), and the resulting molecules were ranked according to favorable geometries and interactions with key binding site residues (e.g., D121$^{3.32}$). (F) Representative compounds were tested in binding assays, and active compounds were optimized for potency and affinity through a cycle of analoging, docking, and testing.

Currently, only a few molecules have been mooted as even modestly selective antagonists for the receptor[15,22] and selective agonists have yet to be described. Accordingly, much of what we know about 5-HT$_{5A}$R pharmacology and its (dys)function stems from blockade with the commercially available 5-HT$_{5A}$R antagonist SB-699551.[23] However, SB-699551 possesses a considerable off-target activity (≤1 μM) for many 5-HTR family members and lacks a chemically matched negative control probe with which to control for them. Indeed, the off-target activities of SB-699551 and of another 5-HT$_{5A}$R antagonist A-843277, the latter of which is unavailable commercially, were substantial enough to confound the interpretation of in vivo studies.[24]

To better illuminate the 5-HT$_{5A}$R function, here we deployed an iterative molecular docking and empirical testing strategy, adapted from those successfully used with the understudied receptors GPR65 and GPR68[8] and with MRGPRX2.[9] Docking of >6 million lead-like molecules against a homology model of the receptor initiated an iterative cycle of analoging, docking, and pharmacological testing that ultimately

https://doi.org/10.1021/acs.jmedchem.1c02031
J. Med. Chem. 2022, 65, 4201−4217

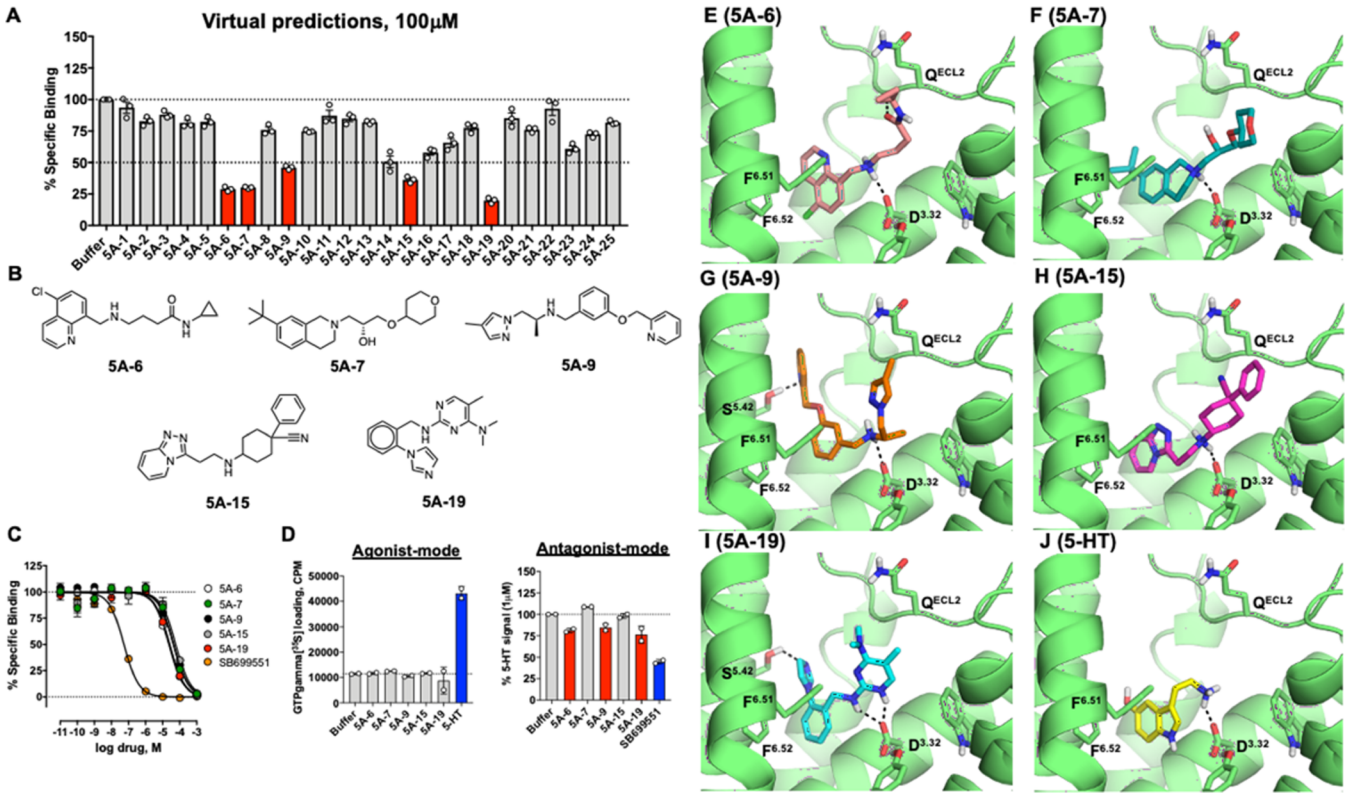

Figure 2. Library docking identifies novel 5-HT$_{5A}$R chemotypes. (A) Single-point competition binding assay of 25 high-ranking docking molecules. At 100 μM, 5 of the 25 (red bars) displaced >50% of the high-affinity agonist [^{3}H]5-CT. Data shown as mean ± standard error of the mean (SEM) (n = 3 in experimental triplicate). (B) Chemical structures of the top five docking hits; each represents a different scaffold. (C) Concentration–response curves of [^{3}H]5-CT displacement by the five docking hits versus the known 5-HT$_{5A}$R antagonist SB-699551. Data are mean ± SEM (n = 3–11 in experimental duplicate). (D) GTPγ[^{35}S] loading assays for agonist (n = 1 in duplicate) and antagonist (n = 2 in triplicate) activities of five docking hits at 32 and 100 μM, respectively. Data shown are mean ± standard deviation (SD). Docked poses of compounds **5A-6** (E), **5A-7** (F), **5A-9** (G), **5A-15** (H), **5A-19** (I), and 5-HT (J). The 5-HT$_{5A}$R is shown in green, and compounds are shown as capped sticks with colored carbons. The Ballesteros–Weinstein numbering[34] is shown as superscript.

identified a novel chemical scaffold with a mid-nanomolar affinity for 5-HT$_{5A}$R and a far more restricted off-target profile versus SB-699551. Property-matched probe pairs that controlled for off-target activities were also developed, and the set of probe molecules was used to investigate a previously hypothesized role for the 5-HT$_{5A}$R in neuropathic pain, here in a mouse model. Whereas the techniques used to develop the probe set resemble those used against homology models of GPR68, GPR65,[8] and MRGPRX2,[9] and against receptors with experimental structures like the melatonin,[25] the Sigma2,[26] and MRGPRX4,[27] this study differs from earlier work in that it was necessary to develop not just probe pairs—composed of a lead active and a close analog that was inactive against the targeted receptor—but a larger probe set to control for the key off-targets of the lead active.

RESULTS

Homology Model Generation, Vetting, and In Silico Screening. We used iterative modeling and testing to seek novel ligands selective for the 5-HT$_{5A}$R (Figure 1). Because selective compounds of either class would be useful, we initially did not differentiate between agonists or antagonists. Moreover, as there is no crystal structure publicly available for the 5-HT$_{5A}$R, we first built 1000 homology models based on the 5-HT$_{1B}$R X-ray structure bound to ergotamine (PDB: 4IAQ;[28] HUGO gene name: HTR1B) using Modeller (Figure 1A).[29] The 5-HT$_{1B}$R was chosen because it shares a 34% overall sequence identity with the 5-HT$_{5A}$R and a 49% sequence identity within the transmembrane regions. Ergotamine was retained in the modeling to ensure a ligand-competent orthosteric binding site.

The resulting models were evaluated for their ability to enrich 17 common lead-like 5-HTR agonists and antagonists (IUPHAR[30]) over 1133 property-matched decoys (Figure 1B). The best-performing model by ligand enrichment was further optimized through energy minimization (Figure 1C) and selected for prospective virtual screening (Figure 1D). The best-performing 5-HT$_{5A}$R model was then screened against >6 million "lead-like" molecules (MW: 300–350, Log P: −1 to 3.5) from the ZINC15 database.[31] For many molecules, no successful pose was calculated, while 2 090 248 molecules were docked and scored. Top-ranked docked molecules were advanced if they were topologically dissimilar to ∼28 000 known aminergic ligands curated from the ChEMBL database[32] (ECFP4 Tc < 0.40). Finally, the top-ranked 2000 poses were visually inspected for unfavorable features that are sometimes missed by the docking scoring function, especially internal strain in the ligands and the occurrence of ligand hydrogen bond donors that are not complemented by particular receptor acceptors, as described[33] (Figure 1E). Ultimately, 25 compounds, each representing a different chemotype (Table S1), were experimentally tested for binding to the 5-HT$_{5A}$R (Figure 1F).

https://doi.org/10.1021/acs.jmedchem.1c02031
J. Med. Chem. 2022, 65, 4201–4217

Table 1. Optimization of Compound Affinity and Potency for 5-HT_{5A}R

Compound	Structure	Global Rank	Tc to knowns	pKi (95% CI)	Arrestin pEC_{50} E_{max} (% of 5-HT)
1. New binders identified in the primary screen					
5A-6	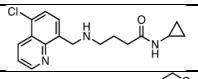	551	0.33	4.94 (4.995 to 4.888)	N.D. N.D.
5A-7	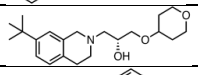	333	0.33	4.67 (4.825 to 4.517)	N.D. N.D.
5A-9	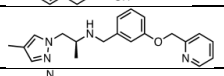	2876	0.39	4.68 (4.783 to 4.569)	N.D. N.D.
5A-15	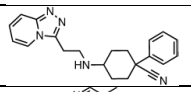	241	0.36	4.54 (4.709 to 4.376)	N.D. N.D.
5A-19	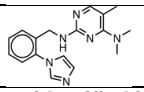	173	0.36	4.89 (5.040 to 4.743)	N.D. N.D.
2. Hit analogues identified in round 1 of optimization					
5A6-1	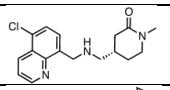	NA	0.34	5.40 (5.551 to 5.247)	N.D. N.D.
5A6-2	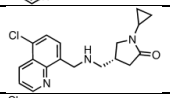	NA	0.31	5.17 (5.360 to 4.983)	N.D. N.D.
5A6-8	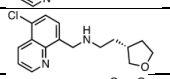	NA	0.33	5.18 (5.319 to 5.029)	N.D. N.D.
5A6-10	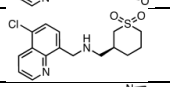	NA	0.29	5.51 (5.639 to 5.386)	N.D. N.D.
5A6-12	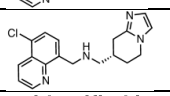	NA	0.34	5.49 (5.665 to 5.328)	N.D. N.D.
2. Hit analogues identified in round 2 of optimization					
5A6-16	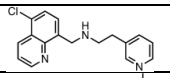	NA	0.32	5.62 (5.852 to 5.394)	N.D. N.D.
5A6-20	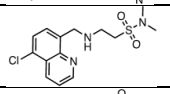	NA	0.32	6.68 (6.765 to 6.602)	N.D. N.D.
5A6-36	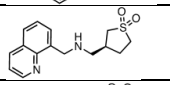	NA	0.32	6.25 (6.324 to 6.166)	N.D. N.D.
5A6-39	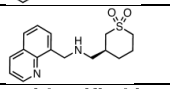	NA	0.33	6.15 (6.211 to 6.089)	N.D. N.D.
2. Hit analogues identified in round 3 of optimization					
5A6-55	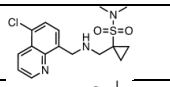	NA	0.30	6.97 (7.042 to 6.899)	N.D. N.D.
5A6-59	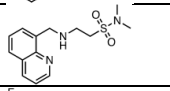	NA	0.32	6.64 (6.807 to 6.479)	N.D. N.D.
5A6-74	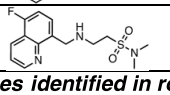	NA	0.29	6.57 (6.704 to 6.434)	N.D. N.D.
2. Hit analogues identified in round 4 of optimization					
5A6-78	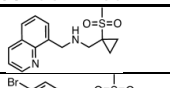	NA	0.32	7.38 (7.479 to 7.283)	6.45 18.3
5A6-84	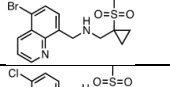	NA	0.29	6.75 (6.876 to 6.633)	N.D. N.D.
5A6-88	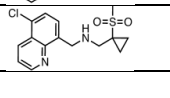	NA	0.28	6.90 (7.036 to 6.755)	5.44 10.5

Iterative Docking and Testing Enable Affinity Maturation of a Novel Quinolone Scaffold. The initial set of 25 docking hits and analogs were tested in binding assays of increasing stringency to probe their interactions with the orthosteric site. Testing at a single concentration of 100 μM identified five chemotypes that displaced >50% of high-affinity

https://doi.org/10.1021/acs.jmedchem.1c02031
J. Med. Chem. 2022, 65, 4201−4217

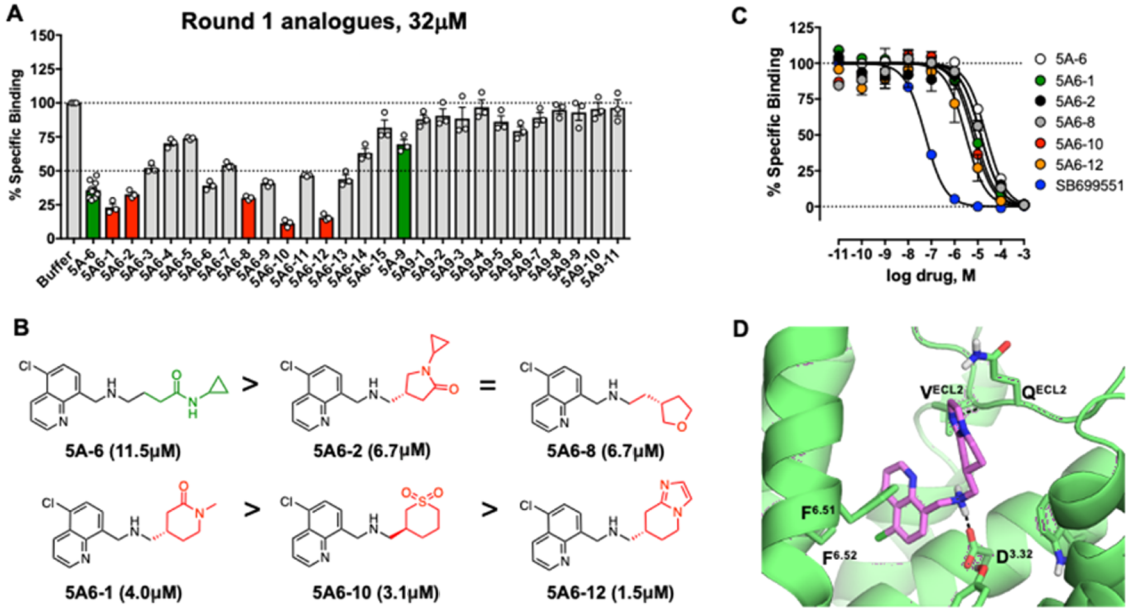

Figure 3. The **5A-6** series is identified as a candidate for optimization in the first round of analoging. (A) Single-point competition binding assay of 15 analogs of compound **5A-6** and 11 analogs of compound **5A-9**. Five of the **5A-6** analogs (red bars) were capable of displacing the binding of the high-affinity agonist [^{3}H]5-CT better than the parent compound **5A-6** (green bar). None of the **5A-9** analogs tested had better affinity than the parent compound (green bar). Each analog was tested at 32 μM. Data shown as mean ± SEM (n = 3 in experimental triplicate). (B) Chemical structures of the five active analogs relative to the parent compound **5A-6**. The variable group in each structure is colored red. Ki values for each molecule are indicated below the structure. (C) Competition binding assays of the five active analogs relative to the parent compound **5A-6** and the known antagonist SB-699551. Data shown as mean ± SEM (n = 3−11 in experimental duplicate). (D) Docked pose of the analog **5A6-12**, which had the greatest improvement in affinity relative to **5A-6**. The 5-HT$_{5A}$R is shown in green, and **5A6-12** is shown as capped sticks with carbons colored pink. The Ballesteros−Weinstein numbering is shown as superscript.

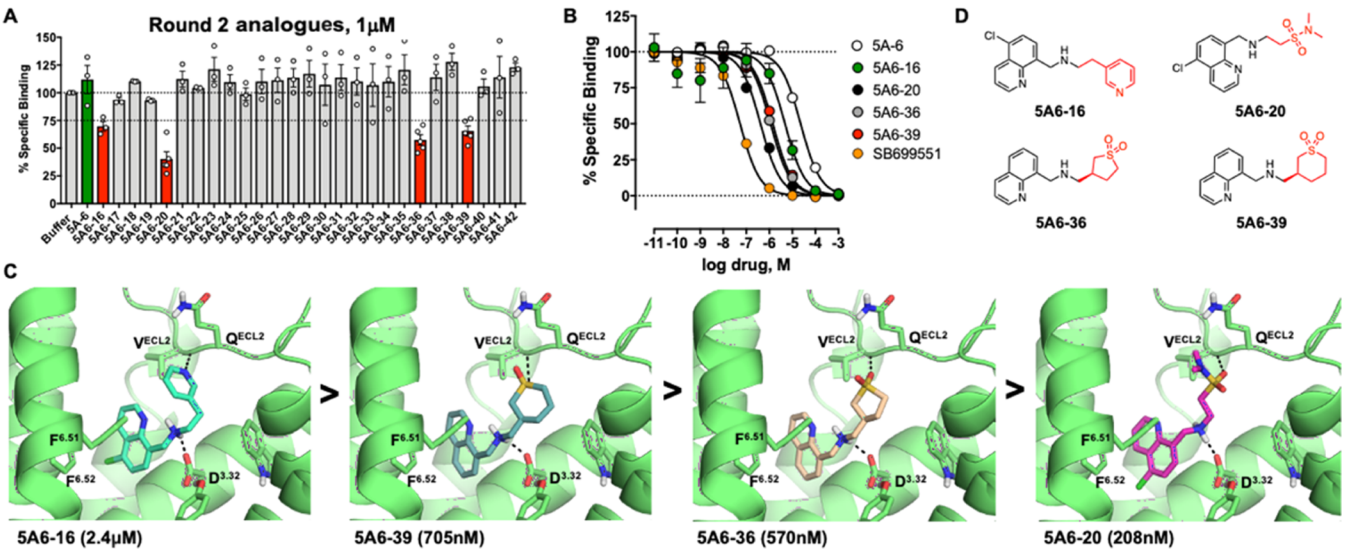

Figure 4. Optimization of chemical features identified in the first round leads to nanomolar ligands. (A) Single-point competition binding assay of 27 analogs. Four of the **5A-6** analogs (red bars) displaced the [^{3}H]5-CT better than the parent compound **5A-6** (green bar). Each analog was tested at 1 μM. Data shown as mean ± SEM (n = 3−5 in experimental triplicate). (B) Competition binding assays of the four active analogs versus the parent **5A-6** and the known antagonist SB-699551. Data shown as mean ± SEM (n = 3−11 in experimental duplicate). (C) Docked poses of the four active analogs (from left to right) **5A-16**, **5A6-39**, **5A6-36**, and **5A6-20**. Ki values are indicated below the image. The 5-HT$_{5A}$R is shown in green, and the molecules are shown as capped sticks with colored carbons. The Ballesteros−Weinstein numbering is shown as superscript. (D) Chemical structures of the four active analogs. The variable group in each structure is colored red.

orthosteric agonist binding ([^{3}H]5-CT) from the human 5-HT$_{5A}$R (Figure 2A,B), corresponding to a 20% hit rate. In competition radioligand binding assays spanning 8 orders of magnitude, the affinities of compounds **5A-6**, **5A-7**, **5A-9**, **5A-15**, and **5A-19** ranged from 12 to 42 μM (Figure 2C and Table 1). Although substantially weaker than the mid-nM antagonist SB-699551, several of these new ligands had an antagonist-like activity in GTP-loading assays (Figure 2D). Based on their potency, target engagement in functional assays, and availability of analogs in the docking library, we sought to

https://doi.org/10.1021/acs.jmedchem.1c02031
J. Med. Chem. 2022, 65, 4201−4217

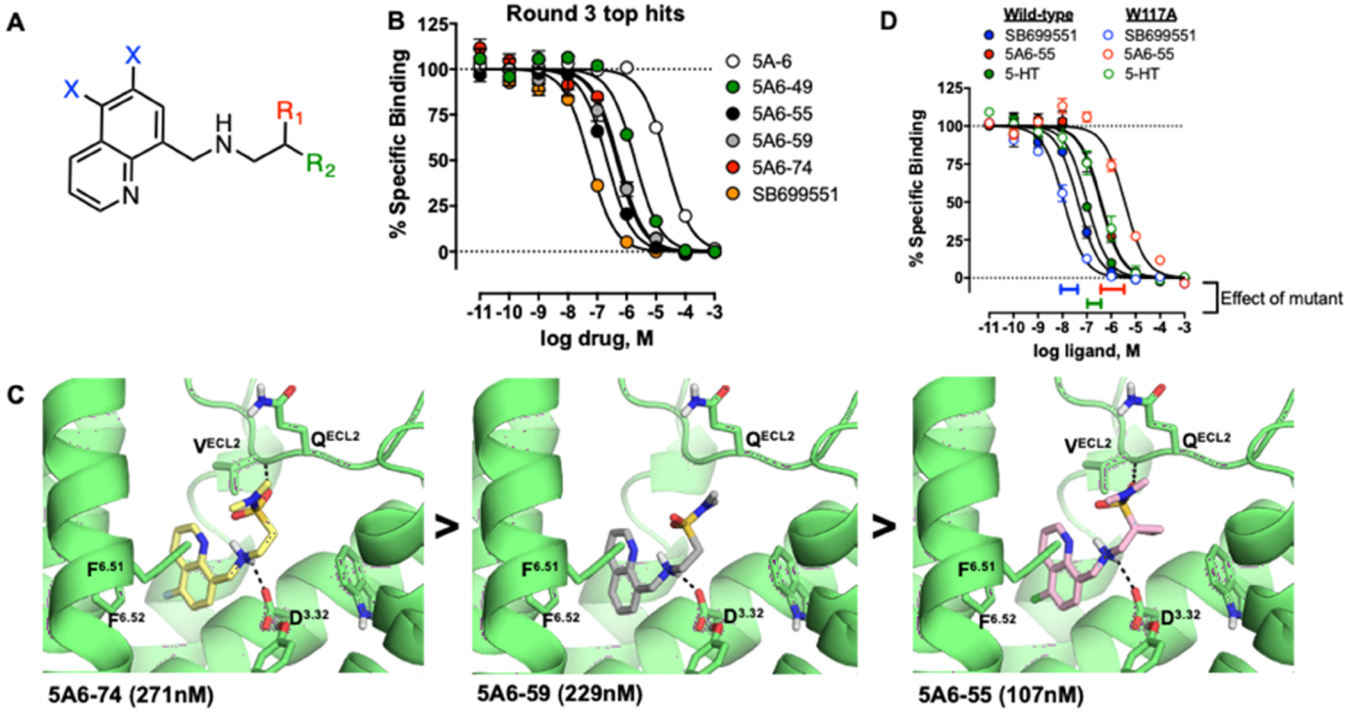

Figure 5. High-affinity binding through sulfonamide substitutions and modeled engagement of ECL2. (A) Three regions (X, R1, R2) targeted in the third round of optimization are highlighted on the structure of the anchor scaffold. (B) Competition binding assays of the four active analogs identified in this round versus parent **5A-6** and the known antagonist SB-699551. Data shown as mean ± SEM (n = 3−11 in experimental duplicate). (C) Docked poses of the three most potent analogs (from left to right) **5A6-74**, **5A6-59**, and **5A6-55**. Ki values are indicated below the image. The 5-HT$_{5A}$R is shown in green, and the molecules are shown as capped sticks with colored carbons. The Ballesteros−Weinstein numbering is shown as superscript. (D) Competition binding assays of **5A6-55**, the known antagonist SB-699551, and the endogenous ligand 5-HT at wild-type 5-HT$_{5A}$R and the single-point mutant W117$^{3.28}$A. Data shown as mean ± SEM (n = 3 in experimental duplicate).

optimize the **5A-6** and **5A-9** scaffolds via a widely used analog-by-catalogue strategy[8,9,36,37] (Figure 2E−J).

Docking of **5A-6** suggested that it interacts with conserved binding site residues including a salt bridge between the ligand's secondary amine and the D121$^{3.32}$—a hallmark interaction between aminergic GPCRs and their ligands—and van der Waals contacts between the ligand's halogenated quinoline and residues on TMs 3, 5, and 6, including C125$^{3.36}$, A208$^{5.46}$, and F302$^{6.52}$ (Figure 2E). The docked pose also featured a new hydrogen bond interaction between the carbonyl group of the terminal ligand amide and the backbone of V194^{ECL2} (extracellular loop 2). Since the left-hand side of **5A-6** coordinates many interactions common among biogenic amine receptors, and to all 5-HTRs in particular[12] (Figure 2J), we mainly explored substitutions on the right-hand side of the molecule that extends toward the extracellular loops. The preliminary docking hit was optimized through several rounds of analoging within the ZINC15 database.[31] In the first round, 4374 analogs were identified by a substructure similarity search using the core scaffold of **5A-6** against the "lead-like" subset of ZINC15. After removing all but the cationic molecules to preserve the D121$^{3.32}$ interaction, these analogs were docked to the 5-HT$_{5A}$R model. Analogs that maintained putative key interactions observed for the parent molecule and that formed additional favorable contacts were selected for experimental testing. Similarly, the docking of compound **5A-9** suggested that it hydrogen-bonds with D121$^{3.32}$ through its cationic nitrogen, as well as with S204$^{5.42}$ (Figure 2G). A set of 2450 topologically similar analogs of **5A-9** were identified, as above, and docked to the 5-HT$_{5A}$R model.

Together, 15 analogs of **5A-6** and 11 analogs of **5A-9** were prioritized for testing. Five analogs of **5A-6** outperformed the parent molecule in single-concentration testing at 32 μM (Figure 3A,B and Table 1). Conversely, none of the **5A-9** analogs exhibited any improvement over the parent and this scaffold was not further pursued. Competition binding assays (Figure 3C) confirmed that **5A-6** analogs with a bulky rigidified ring system on the right-hand side, such as substituted furan (**5A6-8**) or piperidine (**5A6-1**) rings or a cyclic sulfone (**5A6-10**), bound with higher affinity than the parent molecule (Figure 3B). Compound **5A6-12** (1.5 μM) showed the greatest improvement in affinity versus **5A-6** (12 μM) (Figure 3D).

Beneficial chemical features identified in the first round of hit optimization, such as thiane−dioxide (**5A6-10**) and tetra-hydro-imidazo-pyridine (**5A6-12**) groups, were the basis for a second round of analoging. Similarity searches of the ZINC15 database followed by docking yielded a diverse set of 27 analogs (Table S3). Testing in competition radioligand binding assays under 32-fold more stringent conditions (1.0 μM) revealed four analogs with improved affinity (Figure 4A,B and Table 1). Binding affinity increased as much as 55-fold versus the parent molecule; analog rank order affinity (μM to nM): **5A6-16** > **5A6-39** > **5A6-36** > **5A6-20**, with the Ki of **5A6-20** reaching 208 nM. As with round 1, all top analogs of this set docked to hydrogen bond with the backbone amide of V194^{ECL2} (Figure 4C). As exemplified by **5A6-20**, affinity appeared to track with the nature of the sulfonyl variant—a sulfonamide substitution (**5A6-20**) was better than a cyclic sulfone (**5A6-36**/**39**; Figure 4D). Conversely, halogenation of

https://doi.org/10.1021/acs.jmedchem.1c02031
J. Med. Chem. 2022, 65, 4201−4217

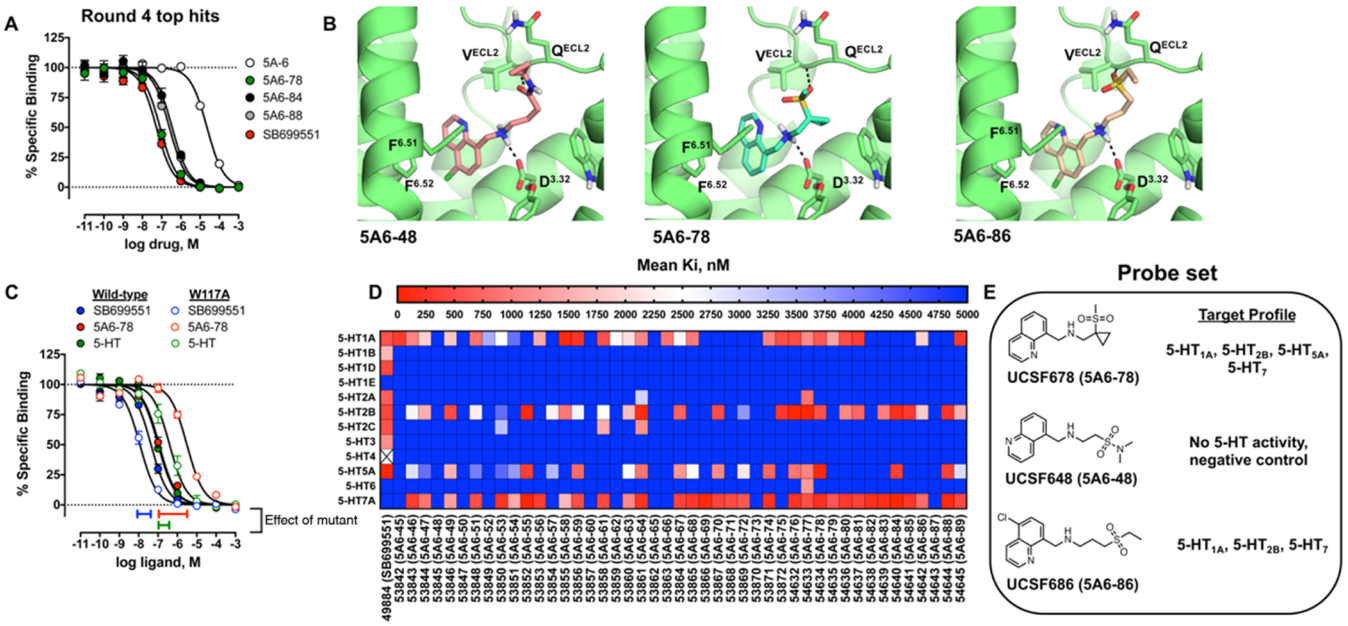

Figure 6. Off-target profile for high-affinity analogs across the 5-HT receptor family and development of a probe set. (A) Competition binding assays of the four most active analogs identified in round 4 of analoging relative to the parent compound **5A-6** and the known antagonist SB-699551. Data shown as mean ± SEM (n = 3−11 in experimental duplicate). (B) Docked poses of the three most potent analogs (from left to right) **5A6-84**, **5A6-88**, and **5A6-78**. Ki values are indicated below the image. The 5-HT_{5A}R is shown in green, and the molecules are shown as capped sticks with colored carbons. The Ballesteros−Weinstein numbering is shown as superscript. (C) Competition binding assays of **5A6-78**, the known antagonist SB-699551, and the endogenous ligand 5-HT at wild type and the single-point mutant $W117^{3.28}A$. Data shown as mean ± SEM (n = 3−6 in experimental duplicate). (D) Affinity panel with Ki values (nM) of analogs from rounds 3 and 4 against all members of the 5-HT receptor family. (E) Target profile of the **UCSF678** probe set.

the quinoline ring reduced affinity, as exemplified by the close analogs **5A6-10** (3.1 μM) and **5A6-39** (705 nM).

Further Lead Optimization and Testing of the Structural Model. Cyclic sulfone and sulfonamide substituents conferred relatively high binding affinity to the quinoline ring and basic amine anchor scaffold, modeled to occur through hydrogen bonds with ECL2 residues (Figure 4C). In round 3, we investigated changes to (i) the type and location of quinoline ring halogenation, including removing the halogen entirely (X); (ii) the configuration of the sulfonamide (R2); (iii) the configuration of the cyclic sulfone (R2); and (iv) the type of hydrogen bond acceptor (R2) (Figure 5A and Table S4). We also explored the addition of hydrophobic substituents (R1). Analogs with a sulfonamide configuration similar to **5A6-20** exhibited the highest affinities (Figure 5B,C and Table 1). Compound **5A6-74** had an affinity similar to **5A6-59**, despite posing to interact with both $D121^{3.32}$ and $V194^{ECL2}$, while **5A6-59** is only modeled to hydrogen-bond with $D121^{3.32}$ alone. This may reflect the unfavorable effect of halogenation on **5A6-74**, an effect that is also apparent in comparing **5A6-10** and **5A6-39** (Figures 3 and 4). Compound **5A6-55**, which had the highest affinity of any analog tested thus far, resembled **5A6-20** but possessed an additional cyclopropyl group that is posed to make apolar contacts with $W117^{3.28}$ and that reorients the sulfonamide hydrogen bond between the main-chain nitrogen of Val^{ECL2} and a sulfonamide oxygen (Figure 5C). The advantages conferred by this cyclopropyl group may have overcome the negative effects of quinoline ring halogenation, which also occurs in **5A6-55**. Consistent with the modeled orientation, the substitution of $W117^{3.28}$ to alanine (W117A) decreased **5A6-55** binding affinity 10-fold, with only a 3.9-fold decrease on the endogenous ligand 5-HT that lacks hydrophobic substitution extending toward $W117^{3.28}$ (Figure 5D). Intriguingly, the widely used antagonist SB-699551 bound threefold better to $W117A^{3.28}$ than to the wild-type receptor (Figure 5D), supporting a different set of interactions and different overall pose within the binding pocket for the much larger SB-699551 versus **5A6-55** and its congeners.

A final round of analogs combined minor changes to the halogenation state of the quinoline with modifications to the sulfone group, to the size and position of the hydrophobic ring, and to the hydrogen bond acceptor (Table S5). Converting the sulfonamide to a methyl-sulfone, retaining the cyclopropyl ring, while dehalogenating the quinoline ring yielded the 41 nM **5A6-78** (Figure 6 and Table 1). Consistent with trends seen throughout the series, bromination (**5A6-84**) and chlorination (**5A6-88**) of the quinoline ring of **5A6-78** at the 6-position decreased affinity by 4.2- and 3.1-fold, respectively (Figure 6B). From the docking poses, these decreases may reflect the loss of a hydrophobic contact with $A208^{5.46}$ on TM5. As with the highly similar analog **5A6-55**, but larger in its overall effect, mutating $W117^{3.28}$ to alanine decreased **5A6-78** binding affinity more than 25-fold (Figure 6C), supporting both an important interaction with this side chain and the docking pose. While $W117^{3.28}$ is fairly conserved among 5-HTR subtypes, it is substituted in 5-HT_{1A}R (Phe), 5-HT_4R (Arg), and 5-HT_7R (Phe) (HUGO gene names: HTR1A, HTR4, and HTR7, respectively).

Comprehensive Affinity Profiling Reveals That the Novel Quinoline/Sulfone Scaffold Confers a More Restricted Binding Profile Than SB-699551. In collaboration with the NIMH Psychoactive Drug Screening Program (PDSP, https://pdspdb.unc.edu/pdspWeb), we comprehensively profiled round 3 and round 4 analogs across 12 5-HTRs, assessing selectivity versus the widely used reagent, SB-699551.

https://doi.org/10.1021/acs.jmedchem.1c02031
J. Med. Chem. 2022, 65, 4201−4217

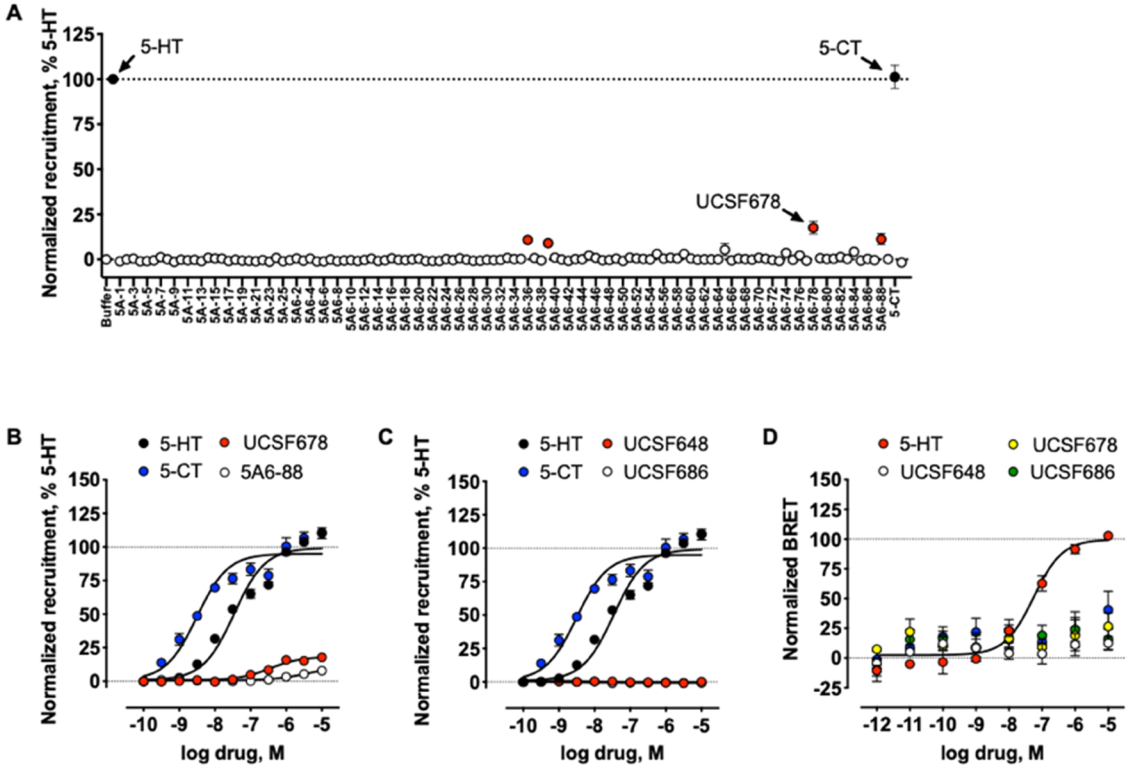

Figure 7. Comprehensive activity profiling reveals that select analogs are arrestin-biased partial agonists. (A) Tango β-arrestin2 recruitment assays[4] testing the activity of initial virtual docking hits and subsequent **5A-6** series analogs at 10 μM at the human 5-HT_{5A}R. Values are normalized to the full agonist serotonin (5-HT, 100%) and presented as mean ± SEM of three to five experiments in quadruplicate. (B, C) The activities of probe molecules **5A6-48**, **5A6-78**, and **5A6-86** for β-arrestin2 recruitment were confirmed by concentration−response curves. Emax values of 5-HT for each plate were calculated via three-parameter logistic fits in GraphPad Prism and used to normalize the raw luminescence values of test ligands. Baseline luminescence values were shared between concentration−response curves on the same 384-well plate. Normalized mean luciferase values (%) were combined across experiments and re-fit to the three-parameter model sharing baseline values. Data shown are mean ± SEM of 4−11 experiments in quadruplicate. (D) Testing activation of the GαoA pathway by probe molecules **UCSF648**, **UCSF678**, and **UCSF686**, and **5A6-88** and the reference full agonist 5-HT. Emax values of 5-HT for each plate were calculated via three-parameter logistic fits in GraphPad Prism and used to normalize the BRET2 ratios of test ligands. Data shown as mean ± SEM (n = 4 in experimental duplicate).

SB-699551 exhibited appreciable affinity (Ki < 2 μM) for many 5-HTR subtypes including 5-HT_{1A}R, 5-HT_{1B}R, 5-HT_{1D}R, 5-HT_{2A}R, 5-HT_{2B}R, 5-HT_{2C}R, and 5-HT_3 (ion channel), in addition to the 5-HT_{5A}R (Figure 6D) (HUGO gene names: HTR1A, HTR1B, HTR1D, HTR2A, HTR2B, HTR2C, and HTR3A, respectively). Conversely, most of our analogs lacked affinity for 5-HT_{1B}R, 5-HT_{1D}R, 5-HT_{2A}R, 5-HT_{2C}R, and 5-HT_3. Unique to our analog series was a gain in affinity for 5-HT_{7A}, which is predicted to have a nearly identical orthosteric binding pocket to 5-HT_{5A}R. Our highest-affinity compound, **5A6-78**, exhibited a marked improvement over SB-699551, with binding restricted to just 5-HT_{1A}R, 5-HT_{2B}R, and 5-HT_{7A}R, in addition to 5-HT_{5A}R (Figure 6D). We will refer to **5A6-78** as **UCSF678** from here on.

To control for the remaining off-target activity of **UCSF678**, we sought molecules that closely resembled **UCSF678** structurally but lacked binding to 5-HT_{5A}R or other off-targets. Such molecules, used in counterpoint to **UCSF678**, can act as "probe pairs" that disentangle the on- from off-target effects of the probe. Two close analogs emerged: **5A6-48** (hereafter referred to as **UCSF648**), which has no measurable effect on any of the 5-HTR receptor subtypes, and **5A6-86** (hereafter referred to as **UCSF686**), which lost affinity at 5-HT_{5A}R (>10 000 nM) but not at 5-HT_{1A}R, 5-HT_{2B}R, and 5-HT_7R (Figure 6E). Docked poses of **UCSF648** suggest that the movement of the quinoline nitrogen across the ring reduces activity by eliminating an internal hydrogen bond with the cationic nitrogen, reducing preorganization. Since the quinoline nitrogen in **UCSF648** does not find a complementary hydrogen bond donor on the receptor, in the docked pose, a desolvation penalty is also likely incurred. For **UCSF686**, SAR suggests that the primary insult for the 5-HT_{5a}-R activity is the introduction of the chloro-group on the quinoline ring, though the size of this effect is greater than in other molecules in this series. Irrespective of the structural origins of these effects, this probe triple of **UCSF678**, **UCSF648**, and **UCSF686** can be used together in seeking phenotypic effects in cells, tissues, or organisms, controlling for the non-5-HTR binding of the series (**UCSF648**) and for the off-target engagement of 5-HT_{1A}R, 5-HT_{2B}R, and 5-HT_{7A}R (**UCSF686**). A comprehensive off-target analysis for these probes can be found in Figure S1.

Weak Partial Agonism and Arrestin Bias of UCSF678, and GPCRome-Wide Activity Profiling. Arrestin recruitment is a sensitive screen for GPCR activity, especially when studying orphan and understudied GPCRs.[4] Here, we tested the initial 25 docking hits and subsequent **5A-6** series analogs for their ability to recruit β-arrestin2 relative to full agonists. Tested at 10 μM (Figure 7A) and confirmed by concentration−response curves (Figure 7B), the analogs **5A6-36**, **5A6-39**, and **UCSF678** were partial agonists for β-arrestin2 recruitment. **UCSF678** had the most robust signal, recruiting

https://doi.org/10.1021/acs.jmedchem.1c02031
J. Med. Chem. 2022, 65, 4201−4217

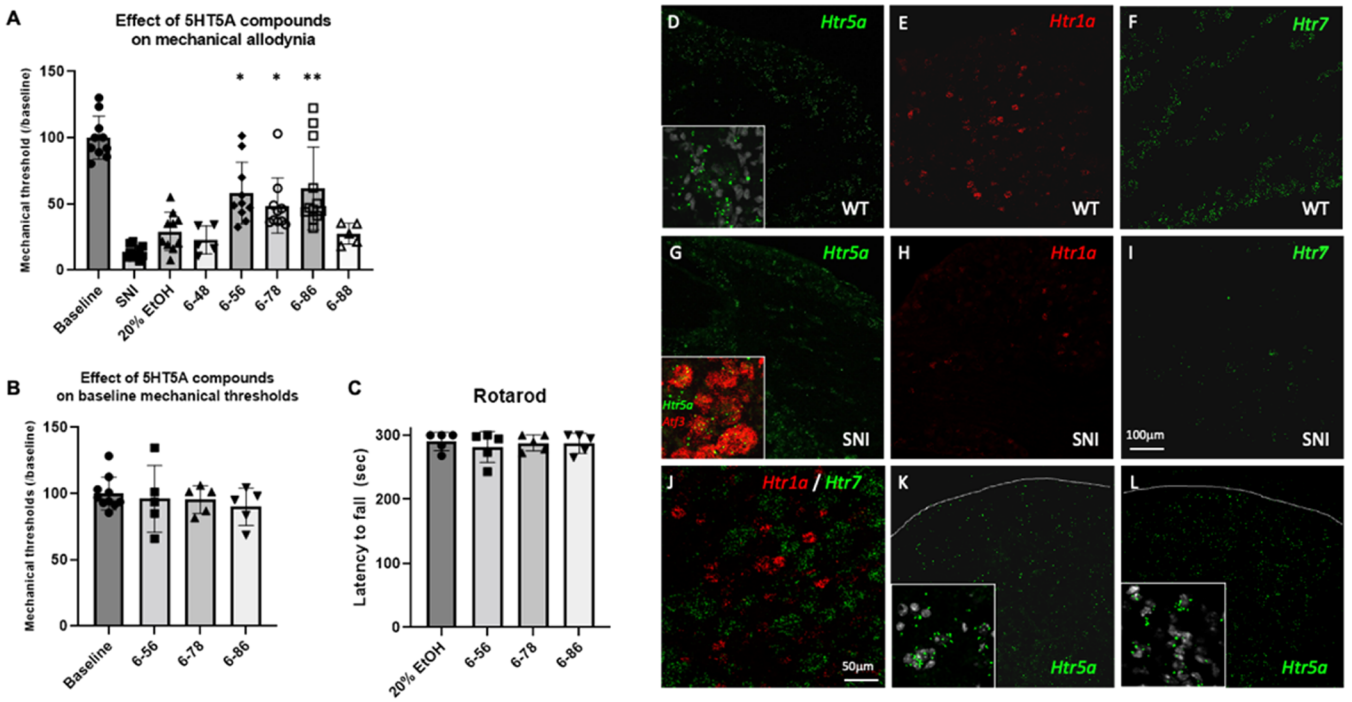

Figure 8. Intrathecal injection of the **5A-6** probe set is antiallodynic. (A) The **5A6-56**, **UCSF678**, and **UCSF686** ligands reduced the mechanical hypersensitivity that develops following sciatic nerve injury (SNI), compared to vehicle (20% ethanol). In contrast, the **UCSF648** and **UCSF688** ligands were ineffective. Data shown are mean ± SEM; one-way ANOVA with Dunnett's multiple comparison post hoc test was performed to compare the effect of the various ligands to the vehicle control (20% ethanol); $*p < 0.05$; $**p < 0.01$. (B, C) None of the ligands tested altered the baseline mechanical thresholds in the absence of an injury (B) or the motor performance in the rotarod test (C). (D–L) In situ hybridization illustrates mRNA coding for the 5-HT receptor subtypes 5A (green (D, G)), 1A (red (E, H, J)), and 7 (green (F, I, J)). These receptors are expressed at various levels in sensory neurons before (D–F) or after (G–I) partial sciatic nerve injury (SNI). Note that the 1A and seven subtypes are expressed in nonoverlapping subsets of dorsal root ganglia (DRG) neurons (J). The 1A and seven (but not 5A) subtypes are downregulated in DRG after SNI. (K–L) The 5-HT$_{5A}$R mRNA is also expressed in the dorsal horn of the spinal cord, both before (K) and after (L) peripheral nerve injury. Scale bar is 100 μm for all panels except (G), where it is 50 μm.

β-arrestin2 to 18% of 5-HT and 5-CT controls. Counter-screens at the Gi/o family transducer GαoA failed to detect activation relative to the 5-HT control (Figure 7C,D), suggesting that **UCSF678** is β-arrestin-biased.

For completeness, we screened the probe set molecules **UCSF648**, **UCSF678**, and **UCSF686** across >300 GPCRs in the Tango assay to detect activation across the GPCRome.[4] We followed up several GPCRome hits in concentration–response curves to reveal that our probe set was largely inactive. Specifically, **UCSF648** weakly activated ADRA2A and MTNR1A (Figure S2A–C), **UCSF686** weakly activated CXCR7 (HUGO gene name: ACKR3; Figure S2D,E), and the probe molecule **UCSF678** activated the D2 dopamine receptor (DRD2) and 5-HT$_{2C}$R (INI isoform) with low potencies (>1.0 μM; Figure S2F–H).

Widely Used Antagonist SB-699551 Has Liabilities as a Chemical Probe. SB-699551 is a tool molecule that, over the last 8 years, has been widely used to investigate the in vivo and cellular roles of the 5-HT$_{5A}$ receptor.[16−18,20,21,24,38−45] Use in these studies is predicated not only on its relative selectivity—now in doubt (Figure 6D)—but also on its behavior in assays. Compared to **UCSF678**, SB-699551 exhibited a near-complete concentration-dependent inhibition of luminescence, as early as 20 min after drug addition, in the absence of stimulation of the 5-HT$_{5A}$ receptor, suggesting that SB-699551 is an inhibitor of the luminescence assay itself (Figure S3). Moreover, bright-field illumination of HEK293T cells treated overnight with high concentrations of SB-699551 suggested extensive cytotoxicity compared to the vehicle control and to **UCSF678**. Since many GPCR assays use luminescence as a proxy for activity (e.g., Tango β-arrestin2 recruitment, BRET2 G protein activation, and GloSensor cAMP), SB-699551 may show antagonist activity against many GPCRs, at least at these concentrations. This is an artifact that has been seen previously in other contexts.[46,47] These results suggest caution in interpreting the activity of this compound in pharmacological studies.

Antinociceptive Behavior of New Chemical Probes. 5-HT$_{5A}$R antagonism has been associated with nociception and/or mechanical hypersensitivity/allodynia in mice;[39,43,45] however, the off-target profiles of previously used antagonists confound ready interpretation. With a probe set that controls for activity at different 5-HTR receptors (Figure 6D), we sought to interrogate the contributions of 5-HT$_{5A}$R and other 5-HTR subtypes to nociception (we note that the 5-HTR human and mouse receptors share an 80–100% sequence identity in their orthosteric sites and that for the 5-HT$_{5A}$R itself, the human and mouse orthologs share a 100% sequence identity). Here, we tested the analgesic properties of our **5A-6** probe set in the context of neuropathic pain via the spared-nerve injury (SNI) model, in which two out of three branches of the sciatic nerve are cut.[48] To selectively investigate the contribution of spinal cord 5-HT$_{5A}$R, we administered ligands intrathecally. Unlike the inactive control probe **UCSF648**, which lacked an effect in the SNI mice (Figure 8A), the intrathecal injection of **UCSF678** or the highly related control

https://doi.org/10.1021/acs.jmedchem.1c02031
J. Med. Chem. 2022, 65, 4201−4217

probe **UCSF686**, which is devoid of 5-HT_{5A}R activity, substantially increased the mechanical thresholds ipsilateral to the injury side versus vehicle (Figure 8). Surprised by these findings, we expanded the study to other probes in our set to verify that 5-HT_{5A}R affinity is indeed nonessential. **5A6-56** exhibited antiallodynic effects comparable to **UCSF678** despite having a binding profile restricted to just the 5-HT_{1A}R and 5-HT_7R (one-way analysis of variance (ANOVA); $p < 0.0001$). Conversely, **5A6-88**, which shares the binding profile of **UCSF678** but lacks 5-HT_{1A}R affinity, was not antiallodynic, consistent with the primacy of the 5-HT_{1A}R in rodent models of pain.[49−52] Interestingly, intrathecal **5A6-56**, **UCSF678**, and **UCSF686** had no visible effect on baseline mechanical thresholds, i.e., in the absence of nerve injury (Figure 8B). Importantly, the intrathecal administration of **5A6-56**, **UCSF678**, and **UCSF686** was devoid of sedating effects on the rotarod test (Figure 8C), indicating that their antiallodynic effects were not the result of motor impairment. Taken together, 5-HT_{5A}R modulation is nonsufficient in a rodent neuropathic pain model when we disentangle the on- from off-target effects of **UCSF678**, highlighting the importance of property-matched control probes.

We used in situ hybridization to confirm that the 5-HT receptor targets of our **5A-6** probe set were expressed at the level of the spinal cord as well as the dorsal root ganglia (DRG), where the cell bodies of the sensory neurons that transmit the "pain" message to the spinal cord reside. Consistent with previous studies,[19,20,53] we found that the 5-HT_{5A} subtype is expressed in a wide variety of spinal cord and DRG neurons (Figure 8). Interestingly, the 5-HT_{1A} and 5-HT_7 subtypes were also expressed in DRG neurons but in nonoverlapping subsets (Figure 8). Furthermore, we found that the expression level of 5-HT_7R decreased dramatically in DRG neurons 7 days after SNI (Figure 8I), whereas 5-HT_{5A}R and 5-HT_{1A}R remained unchanged (Figure 8G,H). Somewhat surprisingly, we could not detect the 5-HT_{2B} receptor subtype in DRG neurons, before or after SNI. Taken together, we conclude that the intrathecal administration of our novel **5A-6** probe set can reduce the mechanical allodynia that develops following peripheral nerve injury, likely via an action at sites that include both the spinal cord and the primary afferent neurons.[54,55]

DISCUSSION

Here, we generated a novel series of 112 compounds from five rounds of iterative docking against a homology model, analoging, and empirical testing. From this approach emerged a 42 nM subtype-selective chemical probe (**UCSF678**) with weak partial agonism and β-arrestin bias against the 5-HT_{5A}R, along with two close analogs, **UCSF648** and **UCSF686**, that together control for off-target effects. Consistent with hit rates for previous GPCR virtual screening campaigns,[7] 20% of the docking predictions were confirmed experimentally, a hit rate that was maintained during increasingly stringent affinity maturation to select for potent and selective compounds.

A goal of the study was to find chemical probes with enhanced selectivity versus the widely used 5-HT_{5A}R antagonist SB-699551. We did not initially screen for selectivity across 5-HTRs; instead, we sought chemically novel scaffolds exemplified by compound **5A-6**, enriching for those that exploited different interactions within the orthosteric pocket. Precedence for this comes from reports that unrelated classes of ligands can bind to the same receptor binding pocket and from library docking campaigns where chemical novelty translates into both subtype and functional selectivity.[37,56] Thus, by advancing a novel quinoline/sulfone scaffold, we hoped to exploit a different set of binding pocket residues that varied in distribution across 5-HTR subtypes. Compared to promiscuous 5-HTR ligands such as serotonin itself, the docked poses of our highest-affinity compounds like **UCSF678** and **5A6-88** extend into the upper regions of the binding pocket. We exploited such modeled interactions to further reduce their off-target activity while also exploiting interactions with a conserved residue ($W117^{3.28}$) for high-affinity binding of **UCSF678** and other analogs (via cyclopropane). While mutagenesis experiments suggest that interactions with this tryptophan are important for affinity, we do note that this residue is conserved at all subtypes except 5-HT_{1A}R (Phe), 5-HT_4R (Arg), and 5-HT_7R (Phe), likely contributing to the off-target binding of our series. Despite this limitation, the chemical novelty of the scaffolds explored led to substantially improved selectivity (Figure 6D).

Using a combination of transcriptomics, mouse genetics, and small molecules, previous studies have begun to illuminate the in vitro pharmacology and in vivo roles of the 5-HT_{5A}R, revealing its potential for clinical targeting in CNS diseases and pain (see refs 13 and 15 for review). However, many of these studies used SB-699551 as a "selective" 5-HT_{5A}R antagonist. This is understandable as it was a readily accessible, best-in-class molecule. Here, we find that SB-699551 has liabilities as a chemical probe: it has substantial affinity for many 5-HTRs (Figure 6D), lacks inactive property-matched controls, artifactually decreases assay luminescence, and appears cytotoxic at relevant concentrations. This can have important repercussions both in vitro and in vivo. For instance, the Kassai et al. study revealed that SB-699551 caused sedation that confounded interpretation of its anxiolytic effect. Two other antagonists, ASP5736 and A-843277, are reported to be selective enough for assigning 5-HT_{5A}R function in animal models.[24,57,58] However, neither antagonist is readily accessible and neither is controlled by a "probe pair" for inevitable off-target activities. Meanwhile, **UCSF678** has (i) an affinity for 5-HT_{5A}R resembling that of the previous molecules (42 nM; Figure 6A), (ii) a more restricted off-target profile across 5-HTRs (Figures 6D and 7) and >300 GPCRs (Figure 8), (iii) no cytotoxicity or assay interference (Figure S3), and (iv) "probe pair" molecules with which to control for its off-target activities (Figure 6E). Accordingly, we are making the "probe triple" of **UCSF678**, **UCSF648**, and **UCSF686** readily available to the community, via the Millipore-Sigma probe collection (registry numbers: SML3246 (**UCSF678**), SML3247 (**UCSF648**), and SML3248 (**UCSF686**)).

Our in vivo studies highlight the usefulness of property-matched probe pair molecules for disentangling the on- from off-target effects of chemical probes to correctly assign biological functions to understudied GPCRs. Specifically, our use of **UCSF678** analogs that bind different off-targets previously associated with analgesia (e.g., 5-HT_{1A}R and 5-HT_7R,[59−62] both of which are well precedented for roles in nociception) calls into question the extent to which 5-HT_{5A}R signaling is essential for rodent nociception and/or analgesia. If such experiments were conducted without the full set of control probes used here, a very different conclusion may have been reached. Echoing the arguments of others,[63,64] we suggest that wherever possible, chemical probe sets should be extended to include close analogs that lack activity at the intended target

https://doi.org/10.1021/acs.jmedchem.1c02031
J. Med. Chem. 2022, 65, 4201−4217

but retain off-target activities of the lead probe. Given that SB-699551 is far more promiscuous and poorly controlled relative to the probes developed here (Figure 6D), previous functions assigned to the 5-HT$_{5A}$R merit reconsideration.

Several caveats merit airing. We do not pretend to have fully investigated the structure−activity around **UCSF678** and its analogs—this is a weakness of the "analog-by-catalogue" approach adopted here, which while being economical is limiting. Other molecules in this series may merit investigation, including the SAR around the quinoline ring, which remains underexplored. Also, while we expect that the in vivo activity of **UCSF678** is via an effective antagonism of the 5-HT$_{5a}$ receptor, a role for its weak partial activation of β-arrestin recruitment cannot be ruled out. Finally, while probe set molecules **UCSF686** and **UCSF648** control for off-targets of the lead **UCSF678**, they have other off-targets of their own, including the Sigma1 and Sigma2 receptors (HUGO gene names: SIGMAR1 and TMEM97, respectively), which have well-precedented roles in nociception.[26,65] Thus, while the probe set controls for off-targets of the lead, **UCSF678**, it is not a completely self-contained set that internally controls for all off-targets of the control molecules in the set.

CONCLUSIONS

The 5-HT$_{5A}$R remains the least understood serotonin receptor, despite its association with multiple CNS disorders and in nociception. Indeed, it could be due to our lack of good pharmacological tools that the receptor has been implicated in quite so many disorders, from motor coordination and control to exploratory behavior and anxiety, neuroendocrine function, learning and memory, emotion, brain development, the psychotropic effects of LSD, sleep, circadian rhythm, bladder function, arterial chemoreception,[13,15] memory stabilization[16] and amnesia,[17] and, investigated here, nociception[39,43,45] and antiallodynia.[20,21] Here, we used iterative rounds of structure-guided docking, pharmacological testing, and optimization to discover a new chemical probe for the 5-HT$_{5A}$R, **UCSF678**, which is substantially more selective than existing 5-HT$_{5A}$R antagonists and better behaved in cell culture and in vitro than existing reagents. We combined this probe with two close analogs that are inactive on the 5-HT$_{5A}$R but control for activity on other 5-HTR subtypes and for other off-targets to which the more general chemotype might bind. Whereas **UCSF678** is active against pain in a mouse model, the activities of the probe triple and of other close analogs—each with different profiles against the 5-HT receptor subtypes—suggest that the 5-HT$_{5A}$R does not have a major role in treating pain but rather this flows from other serotonergic receptors, likely the 5-HT$_{1A}$R. As with other chemical probes for understudied GPCRs,[8,9] these molecules will help to more accurately assign biological functions to these targets. More broadly, the close cycle of modeling, docking, and in vitro pharmacology used here may find broad utility in the field. To that end, we make the docking libraries on which we drew (http://zinc15.docking.org and http://zinc.20.docking.org), the cell constructs and assays used for the in vitro pharmacology, and the 5-HT$_{5A}$R probe triple (Millipore-Sigma registry numbers: SML3246 (**UCSF678**), SML3247 (**UCSF648**), and SML3248 (**UCSF686**)) openly available to the community.

MATERIALS AND METHODS

Homology Modeling. A homology model of the 5-HT$_{5A}$R was calculated using the crystal structure of 5-HT$_{1B}$R in complex with ergotamine as the template (PDB: 4IAR (chain A), 4IAQ (chain A)).[28] The sequence of the target, template, and several members of the 5-HTR family were aligned using PROMALS3D,[66] using sequences of human 5-HT$_{1B}$R (Uniprot accession number: P28222), 5-HT$_{2A}$R (P28223), and 5-HT$_{2B}$R (P41595). The alignment was manually edited to (1) remove 31 residues from the amino terminus of 5-HT$_{5A}$R and one residue from the carboxy terminus that extended past the resolved template structure; (2) remove the engineered apocytochrome b562 RIL (BRIL) from the template and the corresponding residues in ICL3 of 5-HT$_{5A}$R. The final sequence alignment is shown in Figure 1A. Based on this alignment, 1000 homology models were built using MODELER-9v15.[29] Ergotamine was retained in the modeling to ensure a ligand-competent orthosteric site. The resulting models were evaluated for their ability to enrich known 5-HT$_{5A}$R ligands over property-matched decoys through docking to the orthosteric site using DOCK3.7[35] (below). Decoy molecules share the physical properties of known ligands but are topologically distinct from them and so are unlikely to bind, thus controlling for the enrichment of molecules by physical properties alone. For this aim, 17 known 5-HT$_{5A}$R ligands with MW <450 were extracted from the IUPHAR database,[67] and 1133 property-matched decoys were generated using the DUD-E server.[68] The 1000 homology models were ranked by their ability to highly enrich the known ligands over the decoy molecules using adjusted log AUC[68] and the enrichment factor at 1% of the database (EF$_{1\%}$), both of which bias for early enrichment and by the fidelity of the docked pose of ergotamine to the crystallographic structure in the template structure. The best scoring model was further optimized through minimization with the AMBER protein force field and the GAFF ligand force field supplemented with AM1BCC charges.[69] The integrity of the minimized model was assessed by redocking the known ligands and decoy molecules and recalculating enrichment factors.

Virtual Ligand Screening and Selection of Potential Ligands for Experimental Testing. The orthosteric site of the 5-HT$_{5A}$R model was prospectively screened against >6 million "lead-like" molecules from the ZINC15 database (http://zinc15.docking.org/) using DOCK3.7.[35] DOCK3.7 fits pregenerated flexible ligands into a binding site by superimposing atoms of each molecule on local hot spots in the site ("matching spheres"), representing favorable positions for individual ligand atoms. Here, 45 matching spheres were used, drawn from the docked pose of lysergic acid diethylamide (LSD). The resulting docked ligand poses were scored by summing the receptor−ligand electrostatics and van der Waals interaction energies and corrected for context-dependent ligand desolvation.[70,71] Receptor structures were protonated using Reduce.[72] Partial charges from the united-atom AMBER[69] force field were used for all receptor atoms. Potential energy grids for the different energy terms of the scoring function were precalculated based on the AMBER potential[69] for the van der Waals term and the Poisson−Boltzmann method QNIFFT[73,74] for electrostatics. Context-dependent ligand desolvation was calculated using an adaptation of the generalized-Born method.[70] Ligands were protonated with Marvin (version 15.11.23.0, ChemAxon, 2015; https://www.chemaxon.com), at pH 7.4. Each protomer was rendered into 3D using Corina (v.3.6.0026, Molecular Networks GmbH; https://www.mn-am.com/products/corina) and conformationally sampled using Omega (v.2.5.1.4, OpenEye Scientific Software; https://www.eyesopen.com/omega). Ligand atomic charges and initial desolvation energies were calculated as described.[31] In the docking screen, each library molecule was sampled in about 16 000 orientations and, on average, 350 conformations. The best scoring configuration for each docked molecule was relaxed by rigid-body minimization. Overall, about 6.11×10^{12} complexes were sampled and scored; this took 3008 core hours—spread over 100 cores, about 30 h of wall-clock time.

https://doi.org/10.1021/acs.jmedchem.1c02031
J. Med. Chem. 2022, 65, 4201−4217

By calculating ECFP4-based Tanimoto coefficients (Tc) against ~28 000 annotated aminergic ligands (acting at dopamine, serotonin, and adrenergic receptors), extracted from the ChEMBL20 database,[32] we filtered the top 3000 ranked molecules emerging from the screen for topological dissimilarity to known ligands. Molecules with Tc < 0.40 to these aminergic ligands were considered as dissimilar and passed this filter. The remaining molecules were visually inspected in their docked poses. Topologically diverse molecules that adopted favorable geometries and formed specific interactions with binding site residues, such as an ion pair with D121$^{3.32}$ and hydrogen bonds with residues on extracellular loop 2 (ECL2), were prioritized from among the top 2000 docking-ranked molecules that remained. Twenty-five compounds were selected for initial experimental testing.

Hit Optimization. Potential analogs of the hit compound **5A-6** (ZINC000089807724) were identified in five iterative rounds through a combination of similarity and substructure searches of the ZINC database.[31] In each iteration, analogs were docked to the 5-HT$_{5A}$R orthosteric site using DOCK3.7. As was true in the primary screen, the resulting docked poses were manually evaluated for specific interactions and compatibility with the site, and prioritized analogs were acquired and tested experimentally.

Compound Handling. All compounds selected for testing were initially >90% pure by high-performance liquid chromatography (HPLC), as reported by the vendors. Compounds were ordered from Sigma-Aldrich, SelleckChem, Cayman Chemical, or Medchem Express. Manually curated hits were purchased from Enamine, Chembridge, and Molport. Portions of each compound (0.5−1 mg) were dissolved in DMSO at 10 mM and maintained as −20 °C stock solutions. Freeze−thaw cycles were minimized, and new stocks of compounds were made from the original dry stocks for additional rounds of binding and activity profiling. All optimized lead compounds were >95% pure by HPLC and ^{1}H NMR from enamine (Figures S4−S9).

Molecular Biology and Site-Directed Mutagenesis. An in-frame fusion between the human 5-HT$_{5A}$R from the Presto-Tango cDNA library and the human Gαi1 was made via HiFi DNA assembly (New England Biolabs, Ipswich, MA). Mutations of key contact points between docked ligands and the human 5-HT$_{5A}$R binding pocket were made via site-directed mutagenesis as directed (Stratagene, La Jolla, CA). Quickchange II mutagenic primer sets were the following: W117A 5-HT$_{5A}$R: 5′aaagtacgtcacatgcaatcgccaactgacaaagtcttcgtc-3′ and 5′-gacgaagactttgtcagttggcgattgcatgtgacgtacttt-3′. Q193A 5-HT$_{5A}$R: 5′-ggctcccgactgaccgcgcattcctctgatcc-3′, 5′-ggatcagaggaatgcgcggtcagtcgggagcc-3′. Q193L 5-HT5A: 5′-aaggctcccgactgacaaggcattcctctgatcc-3′, 5′-ggatcagaggaatgccttgtcagtcgggagcctt-3′. Q193F 5-HT$_{5A}$R: 5′-gaaggctcccgactgacgaagcattcctctgatccct-3′, 5′-agggatcagaggaatgcttcgtcagtcgggagccttc-3′. Individual clones were selected and sequence-verified (GeneWiz, Morrisville, NC).

Cell Culture. To generate membranes expressing high amounts of receptor, suspension Expi293F cells were cultured and transfected exactly as stated by the manufacturer (ThermoFisher Scientific, Waltham, MA). Briefly, Expi293F cells were maintained in vented 125 mL polycarbonate Erlenmeyer flasks (GeneMate, Radnor, PA) in 30 mL of Expi293 growth medium at 37 °C, 8% CO_2, and 115 rpm. For BRET2 functional studies, HEK293T cells obtained from ATCC (Manassas, VA) were maintained in Dulbecco's modified Eagle's medium (DMEM) containing 10% fetal bovine serum (FBS), 100 U/mL penicillin, and 100 μg/mL streptomycin (Gibco-ThermoFisher, Waltham, MA) in a humidified atmosphere at 37 °C and 5% CO_2. For transfection and BRET2 assays, HEKT cells were split into DMEM containing 1% dialyzed FBS, 100 U/mL penicillin, and 100 μg/mL streptomycin (see the BRET2 Functional Assays section) to minimize exposure to 5-HT in serum. For Tango assays that also include GPCRome screens, HTLA cells (a HEK293 cell line stably expressing the tTA-dependent luciferase reporter) and the β-arrestin2-TEV fusion protein (a gift from the laboratory of R. Axel) were maintained in DMEM supplemented with 10% FBS, 100 U/mL penicillin, 100 μg/mL streptomycin, 2.0 μg/mL puromycin, and 100 μg/mL hygromycin B in a humidified atmosphere at 37 °C and 5% CO_2. For transfection and Tango assays, HTLA cells were cultured in DMEM containing 1% dialyzed FBS, 100 U/mL penicillin, and 100 μg/mL streptomycin.

BRET2 Functional Assays. Cells were plated in 6-well dishes at a density of 700 000−800 000 cells/well or in 10 cm dishes at a density of 7−8 million cells/dish. Cells were transfected 2−4 h later using a 1:1:1:1 DNA ratio of receptor/Gα-RLuc8/Gβ/Gγ-GFP2.[75] DNA amounts were 100 and 750 ng per construct for six-well and 10 cm dishes, respectively. Transit 2020 (Mirus Biosciences, Madison, WI) was used to complex the DNA at a ratio of 3.0 μL transit/μg DNA in OptiMEM (10 ng DNA/μL OptiMEM, Gibco-ThermoFisher, Waltham, MA). The next day, cells were harvested from the plate using Versene solution (phosphate-buffered saline buffer + 0.5 mM ethylenediaminetetraacetic acid (EDTA), pH 7.4) and plated in poly-L-lysine-coated white-wall, clear-bottom 96-well assay plates (Greiner Bio-One, Monroe, NC) at a density of 30 000−50 000 cells/well. One day after plating, white backings (PerkinElmer, Waltham, MA) were applied to the plate bottoms, and growth medium was carefully aspirated and replaced with 60 μL of assay buffer (1× Hanks' balanced salt solution (HBSS) + 20 mM *N*-(2-hydroxyethyl)-piperazine-*N*′-ethanesulfonic acid (HEPES), pH 7.4). Ten microliters of freshly prepared 50 μM coelenterazine 400a (Nanolight Technologies, Pinetop, AZ) was added to each well; 5 min later, cells were treated with 30 μL of the drug. Plates were read 5 min later on an LB940 Mithras plate reader (Berthold Technologies, Oak Ridge, TN) with 395 nm (RLuc8-coelenterazine 400a) and 510 nm (GFP2) emission filters at 1 s/well integration times. Plates were read serially six times, and stable measurements from the fourth read were used in all analyses. The BRET2 ratio was computed as the ratio of GFP2 emission to RLuc8 emission.

Tango β-Arrestin2 Recruitment Assay. For analog screening, HTLA cells were plated on day 1 at a density of 10×10^6 cells per 150 mm cell culture dish and transfected with 20 μg Tango receptor cDNA[76] via the calcium phosphate method the following day (day 2).[4,77] Twenty-four hours post transfection (day 3), cells were plated into white-wall, clear-bottom 384-well plates (Greiner Bio-One, Monroe, NC) at 15 000 cells per well in 40 μL DMEM containing 1% dialyzed FBS, 100 U/mL penicillin, and 100 μg/mL streptomycin. Twenty-four hours later (day 4), cells were treated with 20 μL of a single maximal concentration (10 μM) or a ligand serial dilution in assay buffer (20 mM HEPES, 1× HBSS, 0.1% fatty acid-free bovine serum albumin (BSA), 0.01% ascorbic acid, pH 7.4). Approximately 18−20 h later (day 5), 20 μL of a 1/5th diluted solution of Bright-Glo reagent (Promega, Madison, WI) was added directly to the wells, incubated for 10 min at room temperature (RT), light-adapted for 30 s, and read for 0.5 s per well in a Spectramax luminescence plate reader (Molecular Devices, San Jose, CA).

GPCRome-wide screening was accomplished using previously described methods with several modifications.[4] First, HTLA cells were plated in DMEM containing 2% dialyzed FBS, 100 U/mL penicillin, and 100 μg/mL streptomycin. Next, the cells were transfected using an in-plate polyethylenimine (PEI) method.[78] Tango receptor DNAs were resuspended in OptiMEM and hybridized with PEI prior to dilution and distribution into 384-well plates and subsequent addition to cells. After overnight incubation, drugs diluted in DMEM with 1% dialyzed FBS were added to cells without replacement of the medium. Approximately 18−20 h later, luciferin substrate was added, and luminescence was measured as detailed above.

Membrane Preparation. Membranes for radioligand binding and GTPγ[^{35}S] loading experiments were prepared via differential centrifugation as follows. Expi293F suspension cells were split at a density of 75×10^6 cells in 25.5 mL of growth medium and transfected with a DNA complexation mixture containing 30 μg of 5-HT$_{5A}$R (for binding) or 5-HT$_{5A}$R-Gi1 fusion cDNA (for GTPγ[^{35}S] loading), 80 μL of expifectamine, and 3 mL of OptiMEM. Approximately 18 h post transfection, enhancers 1 and 2 were added. Cells were harvested 48 h post transfection via centrifugation at 200*g* for 10 min at 4 °C. The cell pellet was resuspended in 10 mL of homogenization buffer (50 mM Tris−HCl, 2 mM EDTA, and protease inhibitors 500 μM AEBSF, 1.0 μM E-64, 1.0 μM leupeptin,

https://doi.org/10.1021/acs.jmedchem.1c02031
J. Med. Chem. 2022, 65, 4201−4217

150 nM aprotinin; pH 7.4) and dounce-homogenized on ice. Cell debris was removed at 500*g* for 10 min at 4 °C, and microsomes were recovered from the low-speed supernatant at 35 000*g* for 60 min at 4 °C. The high-speed pellet was resuspended in a 0.5−1.0 mL resuspension buffer (50 mM Tris−HCl, 2 mM EDTA, 10 mM $MgCl_2$, 5% glycerol, and protease inhibitors 500 μM AEBSF, 1.0 μM E-64, 1 μM leupeptin, 150 nM aprotinin; pH 7.4) and aliquoted into 1.5 mL tubes. For GTPγ[^{35}S] loading assays, the microsome suspension was immediately frozen and stored at −80 °C. For binding, microsomes were recovered at 16 000*g* for 15 min at 4 °C, followed by removal of the supernatant and storage of the pellet at −80 °C.

Radioligand Binding Assays. The affinities of reference standards and test compounds were determined via conventional competition and saturation radioligand binding assays. Competition assays were performed in round-bottom 96-well plates (Greiner) using standard binding buffer (50 mM Tris−HCl, 10 mM $MgCl_2$, 0.1 mM EDTA, 0.1% fatty acid-free BSA, 1 mM ascorbic acid, pH 7.4) containing 3 nM [^{3}H]5-CT (44−158 Ci/mmol, PerkinElmer, Waltham, MA), serial dilutions of competitor (100 μM to 0.01 nM), and purified wild-type and mutant membranes. Pseudo-first-order assumptions were met using membranes at concentrations that bound ≪10% of the radioligand added to each well. Nonspecific binding was determined in the presence of 10 μM SB-699551. Plates were incubated in the dark for 2 h at RT, and a PerkinElmer Filtermate harvester was used to collect membranes onto 0.3% PEI-treated GF/B glass fiber filtermats that were washed 4× with cold harvest buffer (50 mM Tris−HCl, pH 7.4 at 4 °C). The filters were dried, permeated with Meltilex scintillant (PerkinElmer, Waltham, MA), and counted on a Microbeta plate reader at 1 min/well. Saturation binding assays were performed as above except that a serial dilution of [^{3}H]5-CT (0.1−25 nM) was used. Bound cpm from competition experiments was analyzed in Prism (GraphPad Prism, San Diego, CA) using the Cheng−Prusoff correction to yield Ki equilibrium binding estimates. Equilibrium dissociation constants (K_D) were fit directly from specific binding values using a one-site saturation model in Prism. Selectivity screens by the NIMH Psychoactive Drug Screening Program (PDSP) were performed as described.[5] Validation assays for 5-HT_{5A}R-Gi_1 expression were performed as described above using 10 nM [^{3}H]-LSD (82.4 Ci/mmol, PerkinElmer, Waltham, MA).

GTPγ[^{35}S] Loading Assay. GTPγ[^{35}S] assays were performed in 96-well plates in assay buffer (20 mM HEPES, 100 mM NaCl, 10 mM $MgCl_2$, 1 mM EDTA, 1 mM dithiothreitol (DTT); pH 7.4) containing 10 μM GDP, 10 μM GTPγS (only for nonspecific binding), 0.3 nM GTPγ[^{35}S] (1250 Ci/mmol, PerkinElmer, Waltham, MA), and test or control ligands. In agonist mode, all ligands were screened at 32 μM. In antagonist mode, test ligands (100 μM) or control (10 μM SB-699551) were preincubated with a receptor for 15−30 min at RT before an EC_{80} of 5-HT (1.0 μM) was added. GTP loading was initiated by the addition of a premixture of cell membranes and WGA-SPA PVT beads (PerkinElmer, Waltham, MA) to a final concentration of 0.25 mg beads/well and 15 000 cpm 5-HT_{5A}R-Gi_1/well (as determined by [^{3}H]-LSD binding). Plates were sealed and agitated at RT for 3 h (agonist mode) and 3−5 h (antagonist mode). Plates were counted in SPA mode in a PerkinElmer TriLux microbeta. Results (CPM) were normalized to 5-HT response in GraphPad Prism 5.0.

Animals. Animal experiments were approved by the UCSF Institutional Animal Care and Use Committee and were conducted in accordance with the NIH Guide for the Care and Use of Laboratory animals. Adult (8−10 weeks old) male C56BL/6 mice were purchased from the Jackson Laboratory (strain #664). Mice were housed in cages on a standard 12:12 h light/dark cycle with food and water ad libitum.

Behavioral Analyses. All ligands were dissolved in 20% ethanol at the desired concentration. For all behavioral tests, the experimenter was always blind to treatment. Animals were first habituated for 1 h in Plexiglas cylinders and then tested 30 minutes after intrathecal (spinal cord CSF) injection of the compounds. Hindpaw mechanical thresholds were determined with von Frey filaments using the up-down method.[79] We tested 10 mice per compound, with the exception of 6−48 and 6−88, in which five mice per group were tested. For the ambulatory (rotarod) test, five mice per group were first trained on an accelerating rotating rod, three times for 5 min, before testing with any compound.

Spared-Nerve Injury (SNI) Model of Neuropathic Pain. Two of the three branches of the sciatic nerve were ligated and transected distally under isoflurane anesthesia, leaving the sural nerve intact. Behavior was tested 7−14 days after injury. For most compounds, we tested 10 mice per group; for two compounds, we tested five mice per group.

In Situ Hybridization. In situ hybridization was performed as previously described,[80] 1 week post SNI, using fresh DRG tissues from three adult mice (8−10 week old) and following the Advanced Cell Diagnostics' protocol. This number of mice examined is based on our previous studies demonstrating that patterns of expression are readily and consistently defined with a minimum of three mice. All images were taken on an LSM 700 confocal microscope (Zeiss) and acquired with ZEN 2010 (Zeiss). Adjustment of brightness/contrast and introducing artificial colors (LUT) were done with Photoshop. The same imaging parameters and adjustments were used for all images within an experiment.

Statistical Analyses. All statistical analyses were performed with Prism (GraphPad) using one-way ANOVA with Dunnett's multiple comparison post hoc test. Anatomical and behavioral data are reported as mean ± SEM.

■ ASSOCIATED CONTENT

Supporting Information

The Supporting Information is available free of charge at https://pubs.acs.org/doi/10.1021/acs.jmedchem.1c02031.

CSV file listing compounds, their molecular formula strings, and biological activities (CSV)

PDB-formatted file containing the homology-modeled structure of the 5HT5a receptor used for docking (PDB)

Expanded off-target engagement screen for probe set molecules across human and rodent receptors, channels, and transporters; comprehensive GPCRome profiling of probe set molecules; assay interference by the commercially available antagonist SB-699551; docking hits tested at 5-HT5A receptor; round 1 analogs of compounds **5A-6** and **5A-9** tested at the 5-HT5A receptor; round 2 analogs tested at the 5-HT5A receptor; round 3 analogs tested at the 5-HT5A receptor; round 4 analogs tested at the 5-HT5A receptor (PDF)

■ AUTHOR INFORMATION

Corresponding Authors

Allan I. Basbaum − *Department of Anatomy, University of California, San Francisco, San Francisco, California 94143, United States*; Email: allan.basbaum@ucsf.edu

Bryan L. Roth − *Department of Pharmacology, School of Medicine, University of North Carolina, Chapel Hill, Chapel Hill, North Carolina 27514, United States; National Institute of Mental Health Psychoactive Drug Screening Program, School of Medicine and Division of Chemical Biology and Medicinal Chemistry, Eshelman School of Pharmacy, University of North Carolina, Chapel Hill, Chapel Hill, North Carolina 27514, United States;* orcid.org/0000-0002-0561-6520; Email: bryan_roth@med.unc.edu

Brian K. Shoichet − *Department of Pharmaceutical Chemistry, University of California, San Francisco, San*

https://doi.org/10.1021/acs.jmedchem.1c02031
J. Med. Chem. 2022, 65, 4201−4217

Francisco, California 94143, United States; orcid.org/0000-0002-6098-7367; Email: bshoichet@gmail.com

Authors

Anat Levit Kaplan − *Department of Pharmaceutical Chemistry, University of California, San Francisco, San Francisco, California 94143, United States*

Ryan T. Strachan − *Department of Pharmacology, School of Medicine, University of North Carolina, Chapel Hill, Chapel Hill, North Carolina 27514, United States*

Joao M. Braz − *Department of Anatomy, University of California, San Francisco, San Francisco, California 94143, United States*

Veronica Craik − *Department of Anatomy, University of California, San Francisco, San Francisco, California 94143, United States*

Samuel Slocum − *National Institute of Mental Health Psychoactive Drug Screening Program, School of Medicine, University of North Carolina, Chapel Hill, Chapel Hill, North Carolina 27514, United States*

Thomas Mangano − *National Institute of Mental Health Psychoactive Drug Screening Program, School of Medicine, University of North Carolina, Chapel Hill, Chapel Hill, North Carolina 27514, United States*

Vanessa Amabo − *National Institute of Mental Health Psychoactive Drug Screening Program, School of Medicine, University of North Carolina, Chapel Hill, Chapel Hill, North Carolina 27514, United States*

Henry O'Donnell − *Department of Pharmaceutical Chemistry, University of California, San Francisco, San Francisco, California 94143, United States*

Parnian Lak − *Department of Pharmaceutical Chemistry, University of California, San Francisco, San Francisco, California 94143, United States*

Complete contact information is available at: https://pubs.acs.org/10.1021/acs.jmedchem.1c02031

Author Contributions

#A.L.K., R.T.S. and J.M.B. contributed equally to this work.

Notes

The authors declare no competing financial interest.

■ ACKNOWLEDGMENTS

This work was supported by U.S. NIH grants U24DK1169195 (to B.L.R. and B.K.S.) and R01 MH112205; the NIMH Psychoactive Drug Screening Contract (to B.L.R.); DARPA HR0011-19-2-0020 (to B.K.S., B.L.R., and A.I.B.); R35GM122481 (to B.K.S.); R35NS097306 and Open Philanthropy (to A.I.B.); and K01 MH109943 (to R.T.S.).

■ ABBREVIATIONS USED

5-HT5AR, 5-HT5A receptor; BRIL, apocytochrome b562 RIL; DRG, dorsal root ganglia; ECL2, extracellular loop 2; EF1%, enrichment factor at 1%; K_D, equilibrium dissociation constant; LSD, lysergic acid diethylamide; nM, nanomolar; SNI, sciatic/spared-nerve injury; Tc, Tanimoto coefficients; PDSP, psychoactive drug screening program; PEI, polyethylenimine

■ REFERENCES

(1) Hauser, A. S.; Attwood, M. M.; Rask-Andersen, M.; Schioth, H. B.; Gloriam, D. E. Trends in GPCR drug discovery: new agents, targets and indications. *Nat. Rev. Drug Discovery* **2017**, *16*, 829−842.

(2) Roth, B. L.; Kroeze, W. K. Integrated approaches for genome-wide interrogation of the druggable non-olfactory G protein-coupled receptor superfamily. *J. Biol. Chem.* **2015**, *290*, 19471−19477.

(3) Wacker, D.; Wang, S.; McCorvy, J. D.; Betz, R. M.; Venkatakrishnan, A. J.; Levit, A.; Lansu, K.; Schools, Z. L.; Che, T.; Nichols, D. E.; Shoichet, B. K.; Dror, R. O.; Roth, B. L. Crystal structure of an LSD-bound human serotonin receptor. *Cell* **2017**, *168*, 377.e12−389.e12.

(4) Kroeze, W. K.; Sassano, M. F.; Huang, X. P.; Lansu, K.; McCorvy, J. D.; Giguere, P. M.; Sciaky, N.; Roth, B. L. PRESTO-Tango as an open-source resource for interrogation of the druggable human GPCRome. *Nat. Struct. Mol. Biol.* **2015**, *22*, 362−369.

(5) Besnard, J.; Ruda, G. F.; Setola, V.; Abecassis, K.; Rodriguiz, R. M.; Huang, X. P.; Norval, S.; Sassano, M. F.; Shin, A. I.; Webster, L. A.; Simeons, F. R.; Stojanovski, L.; Prat, A.; Seidah, N. G.; Constam, D. B.; Bickerton, G. R.; Read, K. D.; Wetsel, W. C.; Gilbert, I. H.; Roth, B. L.; Hopkins, A. L. Automated design of ligands to polypharmacological profiles. *Nature* **2012**, *492*, 215−220.

(6) Keiser, M. J.; Setola, V.; Irwin, J. J.; Laggner, C.; Abbas, A. I.; Hufeisen, S. J.; Jensen, N. H.; Kuijer, M. B.; Matos, R. C.; Tran, T. B.; Whaley, R.; Glennon, R. A.; Hert, J.; Thomas, K. L.; Edwards, D. D.; Shoichet, B. K.; Roth, B. L. Predicting new molecular targets for known drugs. *Nature* **2009**, *462*, 175−181.

(7) Roth, B. L.; Irwin, J. J.; Shoichet, B. K. Discovery of new GPCR ligands to illuminate new biology. *Nat. Chem. Biol.* **2017**, *13*, 1143−1151.

(8) Huang, X. P.; Karpiak, J.; Kroeze, W. K.; Zhu, H.; Chen, X.; Moy, S. S.; Saddoris, K. A.; Nikolova, V. D.; Farrell, M. S.; Wang, S.; Mangano, T. J.; Deshpande, D. A.; Jiang, A.; Penn, R. B.; Jin, J.; Koller, B. H.; Kenakin, T.; Shoichet, B. K.; Roth, B. L. Allosteric ligands for the pharmacologically dark receptors GPR68 and GPR65. *Nature* **2015**, *527*, 477−483.

(9) Lansu, K.; Karpiak, J.; Liu, J.; Huang, X. P.; McCorvy, J. D.; Kroeze, W. K.; Che, T.; Nagase, H.; Carroll, F. I.; Jin, J.; Shoichet, B. K.; Roth, B. L. In silico design of novel probes for the atypical opioid receptor MRGPRX2. *Nat. Chem. Biol.* **2017**, *13*, 529−536.

(10) Diaz, C.; Labit-Le Bouteiller, C.; Yvon, S.; Cambon-Kerneis, A.; Roasio, A.; Jamme, M. F.; Aries, A.; Feuillerat, C.; Perret, E.; Guette, F.; Dieu, P.; Miloux, B.; Albene, D.; Hasel, N.; Kaghad, M.; Ferran, E.; Lupker, J.; Ferrara, P. A strategy combining differential low-throughput screening and virtual screening (DLS-VS) accelerating the discovery of new modulators for the orphan GPR34 receptor. *Mol. Inf.* **2013**, *32*, 213−229.

(11) Eberini, I.; Daniele, S.; Parravicini, C.; Sensi, C.; Trincavelli, M. L.; Martini, C.; Abbracchio, M. P. In silico identification of new ligands for GPR17: a promising therapeutic target for neurodegenerative diseases. *J. Comput.-Aided Mol. Des.* **2011**, *25*, 743−752.

(12) McCorvy, J. D.; Roth, B. L. Structure and function of serotonin G protein-coupled receptors. *Pharmacol. Ther.* **2015**, *150*, 129−142.

(13) Volk, B.; Nagy, B. J.; Vas, S.; Kostyalik, D.; Simig, G.; Bagdy, G. Medicinal chemistry of 5-HT5A receptor ligands: a receptor subtype with unique therapeutical potential. *Curr. Top. Med. Chem.* **2010**, *10*, 554−578.

(14) Rees, S.; den Daas, I.; Foord, S.; Goodson, S.; Bull, D.; Kilpatrick, G.; Lee, M. Cloning and characterisation of the human 5-HT5A serotonin receptor. *FEBS Lett.* **1994**, *355*, 242−246.

(15) Thomas, D. R. 5-ht5A receptors as a therapeutic target. *Pharmacol. Ther.* **2006**, *111*, 707−714.

(16) Schmidt, S. D.; Furini, C. R. G.; Zinn, C. G.; Cavalcante, L. E.; Ferreira, F. F.; Behling, J. A. K.; Myskiw, J. C.; Izquierdo, I. Modulation of the consolidation and reconsolidation of fear memory by three different serotonin receptors in hippocampus. *Neurobiol. Learn. Mem.* **2017**, *142*, 48−54.

(17) Aparicio-Nava, L.; Marquez-Garcia, L. A.; Meneses, A. Effects of 5-HT5A receptor blockade on amnesia or forgetting. *Behav. Brain Res.* **2019**, *357*−*358*, 98−103.
(18) Sagi, Y.; Medrihan, L.; George, K.; Barney, M.; McCabe, K. A.; Greengard, P. Emergence of 5-HT5A signaling in parvalbumin neurons mediates delayed antidepressant action. *Mol. Psychiatry* **2020**, *25*, 1191−1201.
(19) Doly, S.; Fischer, J.; Brisorgueil, M. J.; Verge, D.; Conrath, M. 5-HT5A receptor localization in the rat spinal cord suggests a role in nociception and control of pelvic floor musculature. *J. Comp. Neurol.* **2004**, *476*, 316−329.
(20) Avila-Rojas, S. H.; Velazquez-Lagunas, I.; Salinas-Abarca, A. B.; Barragan-Iglesias, P.; Pineda-Farias, J. B.; Granados-Soto, V. Role of spinal 5-HT5A, and 5-HT1A/1B/1D, receptors in neuropathic pain induced by spinal nerve ligation in rats. *Brain Res.* **2015**, *1622*, 377−385.
(21) de los Monteros-Zuñiga, A. E.; Izquierdo, T.; Quinonez-Bastidas, G. N.; Rocha-Gonzalez, H. I.; Godinez-Chaparro, B. Anti-allodynic effect of mangiferin in neuropathic rats: Involvement of nitric oxide-cyclic GMP-ATP sensitive K(+) channels pathway and serotoninergic system. *Pharmacol., Biochem. Behav.* **2016**, *150*−*151*, 190−197.
(22) Peters, J. U.; Lubbers, T.; Alanine, A.; Kolczewski, S.; Blasco, F.; Steward, L. Cyclic guanidines as dual 5-HT5A/5-HT7 receptor ligands: optimising brain penetration. *Bioorg. Med. Chem. Lett.* **2008**, *18*, 262−266.
(23) Corbett, D. F.; Heightman, T. D.; Moss, S. F.; Bromidge, S. M.; Coggon, S. A.; Longley, M. J.; Roa, A. M.; Williams, J. A.; Thomas, D. R. Discovery of a potent and selective 5-ht5A receptor antagonist by high-throughput chemistry. *Bioorg. Med. Chem. Lett.* **2005**, *15*, 4014−4018.
(24) Kassai, F.; Schlumberger, C.; Kedves, R.; Pietraszek, M.; Jatzke, C.; Lendvai, B.; Gyertyan, I.; Danysz, W. Effect of 5-HT5A antagonists in animal models of schizophrenia, anxiety and depression. *Behav. Pharmacol.* **2012**, *23*, 397−406.
(25) Stein, R. M.; Kang, H. J.; McCorvy, J. D.; Glatfelter, G. C.; Jones, A. J.; Che, T.; Slocum, S.; Huang, X. P.; Savych, O.; Moroz, Y. S.; Stauch, B.; Johansson, L. C.; Cherezov, V.; Kenakin, T.; Irwin, J. J.; Shoichet, B. K.; Roth, B. L.; Dubocovich, M. L. Virtual discovery of melatonin receptor ligands to modulate circadian rhythms. *Nature* **2020**, *579*, 609−614.
(26) Alon, A.; Lyu, J.; Braz, J. M.; Tummino, T. A.; Craik, V.; O'Meara, M. J.; Webb, C. M.; Radchenko, D. S.; Moroz, Y. S.; Huang, X. P.; Liu, Y.; Roth, B. L.; Irwin, J. J.; Basbaum, A. I.; Shoichet, B. K.; Kruse, A. C. Structures of the sigma2 receptor enable docking for bioactive ligand discovery. *Nature* **2021**, *600*, 759−764.
(27) Cao, C.; Kang, H. J.; Singh, I.; Chen, H.; Zhang, C.; Ye, W.; Hayes, B. W.; Liu, J.; Gumpper, R. H.; Bender, B. J.; Slocum, S. T.; Krumm, B. E.; Lansu, K.; McCorvy, J. D.; Kroeze, W. K.; English, J. G.; DiBerto, J. F.; Olsen, R. H. J.; Huang, X. P.; Zhang, S.; Liu, Y.; Kim, K.; Karpiak, J.; Jan, L. Y.; Abraham, S. N.; Jin, J.; Shoichet, B. K.; Fay, J. F.; Roth, B. L. Structure, function and pharmacology of human itch GPCRs. *Nature* **2021**, *600*, 170−175.
(28) Wang, C.; Jiang, Y.; Ma, J.; Wu, H.; Wacker, D.; Katritch, V.; Han, G. W.; Liu, W.; Huang, X. P.; Vardy, E.; McCorvy, J. D.; Gao, X.; Zhou, X. E.; Melcher, K.; Zhang, C.; Bai, F.; Yang, H.; Yang, L.; Jiang, H.; Roth, B. L.; Cherezov, V.; Stevens, R. C.; Xu, H. E. Structural basis for molecular recognition at serotonin receptors. *Science* **2013**, *340*, 610−614.
(29) Webb, B.; Sali, A. Comparative protein structure modeling using MODELLER. *Curr. Protoc. Bioinf.* **2014**, *47*, 5.6.1−5.6.32.
(30) Andrade, R.; Barnes, N. M.; Baxter, G.; Bockaert, J.; Branchek, T.; Butler, A.; Cohen, M. L.; Dumuis, A.; Eglen, R. M.; Göthert, M.; Hamblin, M.; Hamon, M.; Hartig, P. R.; Hen, R.; Hensler, J.; Herrick-Davis, K.; Hills, R.; Hoyer, D.; Humphrey, P. P. A.; Latté, K. P.; Maroteaux, L.; Martin, G. R.; Middlemiss, D. N.; Mylecharane, E.; Neumaier, J.; Peroutka, S. J.; Peters, J. A.; Roth, B.; Saxena Pramod, R.; Sharp, T.; Sleight, A.; Villalon, C. M.; Yocca, F. 5-Hydroxytryptamine Receptors (Version 2019.4) in the IUPHAR/BPS Guide to Pharmacology Database. *IUPHAR/BPS Guide to Pharmacology*; Edinburgh University Library, 2019.
(31) Sterling, T.; Irwin, J. J. ZINC 15–Ligand discovery for everyone. *J. Chem. Inf. Model.* **2015**, *55*, 2324−2337.
(32) Gaulton, A.; Hersey, A.; Nowotka, M.; Bento, A. P.; Chambers, J.; Mendez, D.; Mutowo, P.; Atkinson, F.; Bellis, L. J.; Cibrian-Uhalte, E.; Davies, M.; Dedman, N.; Karlsson, A.; Magarinos, M. P.; Overington, J. P.; Papadatos, G.; Smit, I.; Leach, A. R. The ChEMBL database in 2017. *Nucleic Acids Res.* **2017**, *45*, D945−D954.
(33) Irwin, J. J.; Shoichet, B. K. Docking screens for novel ligands conferring new biology. *J. Med. Chem.* **2016**, *59*, 4103−4120.
(34) Ballesteros, J. A.; Weinstein, H. Integrated Methods for the Construction of Three-Dimensional Models and Computational Probing of Structure-Function Relations in G Protein-Coupled Receptors. *Receptor Molecular Biology*; Methods in Neurosciences; Elsevier Inc., 1995; Vol. *25*, pp 366−428.
(35) Coleman, R. G.; Carchia, M.; Sterling, T.; Irwin, J. J.; Shoichet, B. K. Ligand pose and orientational sampling in molecular docking. *PLoS One* **2013**, *8*, No. e75992.
(36) Lyu, J.; Wang, S.; Balius, T. E.; Singh, I.; Levit, A.; Moroz, Y. S.; O'Meara, M. J.; Che, T.; Algaa, E.; Tolmachova, K.; Tolmachev, A. A.; Shoichet, B. K.; Roth, B. L.; Irwin, J. J. Ultra-large library docking for discovering new chemotypes. *Nature* **2019**, *566*, 224−229.
(37) Wang, S.; Wacker, D.; Levit, A.; Che, T.; Betz, R. M.; McCorvy, J. D.; Venkatakrishnan, A. J.; Huang, X. P.; Dror, R. O.; Shoichet, B. K.; Roth, B. L. D4 dopamine receptor high-resolution structures enable the discovery of selective agonists. *Science* **2017**, *358*, 381−386.
(38) Aksu, A. G.; Gunduz, O.; Ulugol, A. Contribution of spinal 5-HT5A receptors to the antinociceptive effects of systemically administered cannabinoid agonist WIN 55,212-2 and morphine. *Can. J. Physiol. Pharmacol.* **2018**, *96*, 618−623.
(39) Cervantes-Durán, C.; Rocha-Gonzalez, H. I.; Granados-Soto, V. Peripheral and spinal 5-HT receptors participate in the pronociceptive and antinociceptive effects of fluoxetine in rats. *Neuroscience* **2013**, *252*, 396−409.
(40) Curtin, P. C.; Medan, V.; Neumeister, H.; Bronson, D. R.; Preuss, T. The 5-HT5A receptor regulates excitability in the auditory startle circuit: functional implications for sensorimotor gating. *J. Neurosci.* **2013**, *33*, 10011−10020.
(41) Gonzalez, R.; Chavez-Pascacio, K.; Meneses, A. Role of 5-HT5A receptors in the consolidation of memory. *Behav. Brain Res.* **2013**, *252*, 246−251.
(42) Mata-Bermudez, A.; Izquierdo, T.; de Los Monteros-Zuniga, E.; Coen, A.; Godinez-Chaparro, B. Antiallodynic effect induced by [6]-gingerol in neuropathic rats is mediated by activation of the serotoninergic system and the nitric oxide-cyclic guanosine monophosphate-adenosine triphosphate-sensitive K(+) channel pathway. *Phytother. Res.* **2018**, *32*, 2520−2530.
(43) Muñoz-Islas, E.; Vidal-Cantu, G. C.; Bravo-Hernandez, M.; Cervantes-Duran, C.; Quinonez-Bastidas, G. N.; Pineda-Farias, J. B.; Barragan-Iglesias, P.; Granados-Soto, V. Spinal 5-HT(5)A receptors mediate 5-HT-induced antinociception in several pain models in rats. *Pharmacol., Biochem. Behav.* **2014**, *120*, 25−32.
(44) Nikiforuk, A.; Holuj, M.; Kos, T.; Popik, P. The effects of a 5-HT5A receptor antagonist in a ketamine-based rat model of cognitive dysfunction and the negative symptoms of schizophrenia. *Neuropharmacology* **2016**, *105*, 351−360.
(45) Vidal-Cantú, G. C.; Jimenez-Hernandez, M.; Rocha-Gonzalez, H. I.; Villalon, C. M.; Granados-Soto, V.; Munoz-Islas, E. Role of 5-HT5A and 5-HT1B/1D receptors in the antinociception produced by ergotamine and valerenic acid in the rat formalin test. *Eur. J. Pharmacol.* **2016**, *781*, 109−116.
(46) Auld, D. S.; Inglese, J. Interferences with Luciferase Reporter Enzymes. In *Assay Guidance Manual*; Markossian, S.; Grossman, A.; Brimacombe, K.; Arkin, M.; Auld, D.; Austin, C. P.; Baell, J.; Chung, T. D. Y.; Coussens, N. P.; Dahlin, J. L.; Devanarayan, V.; Foley, T. L.; Glicksman, M.; Hall, M. D.; Haas, J. V.; Hoare, S. R. J.; Inglese, J.; Iversen, P. W.; Kales, S. C.; Lal-Nag, M.; Li, Z.; McGee, J.; McManus, O.; Riss, T.; Saradjian, P.; Sittampalam, G. S.; Tarselli, M.; Trask, O.

https://doi.org/10.1021/acs.jmedchem.1c02031
J. Med. Chem. 2022, 65, 4201−4217

J., Jr.; Wang, Y.; Weidner, J. R.; Wildey, M. J.; Wilson, K.; Xia, M., Eds.; Eli Lilly & Company and the National Center for Advancing Translational Sciences: Bethesda, MD, 2004.
(47) Thorne, N.; Shen, M.; Lea, W. A.; Simeonov, A.; Lovell, S.; Auld, D. S.; Inglese, J. Firefly luciferase in chemical biology: a compendium of inhibitors, mechanistic evaluation of chemotypes, and suggested use as a reporter. *Chem. Biol.* **2012**, *19*, 1060−1072.
(48) Shields, S. D.; Eckert, W. A., 3rd; Basbaum, A. I. Spared nerve injury model of neuropathic pain in the mouse: a behavioral and anatomic analysis. *J. Pain* **2003**, *4*, 465−470.
(49) Alhaider, A. A.; Wilcox, G. L. Differential roles of 5-hydroxytryptamine1A and 5-hydroxytryptamine1B receptor subtypes in modulating spinal nociceptive transmission in mice. *J. Pharmacol. Exp. Ther.* **1993**, *265*, 378−385.
(50) Fasmer, O. B.; Berge, O. G.; Post, C.; Hole, K. Effects of the putative 5-HT1A receptor agonist 8-OH-2-(di-n-propylamino)tetralin on nociceptive sensitivity in mice. *Pharmacol., Biochem. Behav.* **1986**, *25*, 883−888.
(51) Millan, M. J.; Colpaert, F. C. Attenuation of opioid induced antinociception by 5-HT1A partial agonists in the rat. *Neuropharmacology* **1990**, *29*, 315−318.
(52) Zhang, Y.; Yang, Z.; Gao, X.; Wu, G. The role of 5-hydroxytryptamine1A and 5-hydroxytryptamine1B receptors in modulating spinal nociceptive transmission in normal and carrageenan-injected rats. *Pain* **2001**, *92*, 201−211.
(53) Wu, S.; Zhu, M.; Wang, W.; Wang, Y.; Li, Y.; Yew, D. T. Changes of the expression of 5-HT receptor subtype mRNAs in rat dorsal root ganglion by complete Freund's adjuvant-induced inflammation. *Neurosci. Lett.* **2001**, *307*, 183−186.
(54) Häring, M.; Zeisel, A.; Hochgerner, H.; Rinwa, P.; Jakobsson, J. E. T.; Lonnerberg, P.; La Manno, G.; Sharma, N.; Borgius, L.; Kiehn, O.; Lagerstrom, M. C.; Linnarsson, S.; Ernfors, P. Neuronal atlas of the dorsal horn defines its architecture and links sensory input to transcriptional cell types. *Nat. Neurosci.* **2018**, *21*, 869−880.
(55) Usoskin, D.; Furlan, A.; Islam, S.; Abdo, H.; Lonnerberg, P.; Lou, D.; Hjerling-Leffler, J.; Haeggstrom, J.; Kharchenko, O.; Kharchenko, P. V.; Linnarsson, S.; Ernfors, P. Unbiased classification of sensory neuron types by large-scale single-cell RNA sequencing. *Nat. Neurosci.* **2015**, *18*, 145−153.
(56) Manglik, A.; Lin, H.; Aryal, D. K.; McCorvy, J. D.; Dengler, D.; Corder, G.; Levit, A.; Kling, R. C.; Bernat, V.; Hubner, H.; Huang, X. P.; Sassano, M. F.; Giguere, P. M.; Lober, S.; Da, D.; Scherrer, G.; Kobilka, B. K.; Gmeiner, P.; Roth, B. L.; Shoichet, B. K. Structure-based discovery of opioid analgesics with reduced side effects. *Nature* **2016**, *537*, 185−190.
(57) Yamazaki, M.; Harada, K.; Yamamoto, N.; Yarimizu, J.; Okabe, M.; Shimada, T.; Ni, K.; Matsuoka, N. ASP5736, a novel 5-HT5A receptor antagonist, ameliorates positive symptoms and cognitive impairment in animal models of schizophrenia. *Eur. Neuropsychopharmacol.* **2014**, *24*, 1698−1708.
(58) Yamazaki, M.; Okabe, M.; Yamamoto, N.; Yarimizu, J.; Harada, K. Novel 5-HT5A receptor antagonists ameliorate scopolamine-induced working memory deficit in mice and reference memory impairment in aged rats. *J. Pharmacol. Sci.* **2015**, *127*, 362−369.
(59) Brenchat, A.; Nadal, X.; Romero, L.; Ovalle, S.; Muro, A.; Sanchez-Arroyos, R.; Portillo-Salido, E.; Pujol, M.; Montero, A.; Codony, X.; Burgueno, J.; Zamanillo, D.; Hamon, M.; Maldonado, R.; Vela, J. M. Pharmacological activation of 5-HT7 receptors reduces nerve injury-induced mechanical and thermal hypersensitivity. *Pain* **2010**, *149*, 483−494.
(60) Dogrul, A.; Seyrek, M.; Akgul, E. O.; Cayci, T.; Kahraman, S.; Bolay, H. Systemic paracetamol-induced analgesic and antihyperalgesic effects through activation of descending serotonergic pathways involving spinal 5-HT(7) receptors. *Eur. J. Pharmacol.* **2012**, *677*, 93−101.
(61) Nemmani, K. V.; Mogil, J. S. Serotonin-GABA interactions in the modulation of mu- and kappa-opioid analgesia. *Neuropharmacology* **2003**, *44*, 304−310.
(62) Roca-Vinardell, A.; Ortega-Alvaro, A.; Gibert-Rahola, J.; Mico, J. A. The role of 5-HT1A/B autoreceptors in the antinociceptive effect of systemic administration of acetaminophen. *Anesthesiology* **2003**, *98*, 741−747.
(63) Arrowsmith, C. H.; Audia, J. E.; Austin, C.; Baell, J.; Bennett, J.; Blagg, J.; Bountra, C.; Brennan, P. E.; Brown, P. J.; Bunnage, M. E.; Buser-Doepner, C.; Campbell, R. M.; Carter, A. J.; Cohen, P.; Copeland, R. A.; Cravatt, B.; Dahlin, J. L.; Dhanak, D.; Edwards, A. M.; Frederiksen, M.; Frye, S. V.; Gray, N.; Grimshaw, C. E.; Hepworth, D.; Howe, T.; Huber, K. V.; Jin, J.; Knapp, S.; Kotz, J. D.; Kruger, R. G.; Lowe, D.; Mader, M. M.; Marsden, B.; Mueller-Fahrnow, A.; Muller, S.; O'Hagan, R. C.; Overington, J. P.; Owen, D. R.; Rosenberg, S. H.; Roth, B.; Ross, R.; Schapira, M.; Schreiber, S. L.; Shoichet, B.; Sundstrom, M.; Superti-Furga, G.; Taunton, J.; Toledo-Sherman, L.; Walpole, C.; Walters, M. A.; Willson, T. M.; Workman, P.; Young, R. N.; Zuercher, W. J. The promise and peril of chemical probes. *Nat. Chem. Biol.* **2015**, *11*, 536−541.
(64) Lee, J.; Schapira, M. The promise and peril of chemical probe negative controls. *ACS Chem. Biol.* **2021**, *16*, 579−585.
(65) Sahn, J. J.; Mejia, G. L.; Ray, P. R.; Martin, S. F.; Price, T. J. Sigma 2 receptor/Tmem97 agonists produce long lasting antineuropathic pain effects in mice. *ACS Chem. Neurosci.* **2017**, *8*, 1801−1811.
(66) Pei, J.; Grishin, N. V. Multiple Protein Sequence Alignment Enhanced with Evolutionary and Three-Dimensional Structural Information. *Multiple Sequence Alignment Methods*; Methods in Molecular Biology; Humana Press, 2014; Vol. *1079*, pp 263−271.
(67) Southan, C.; Sharman, J. L.; Benson, H. E.; Faccenda, E.; Pawson, A. J.; Alexander, S. P.; Buneman, O. P.; Davenport, A. P.; McGrath, J. C.; Peters, J. A.; Spedding, M.; Catterall, W. A.; Fabbro, D.; Davies, J. A.; NC-IUPHAR. The IUPHAR/BPS guide to pharmacology in 2016: towards curated quantitative interactions between 1300 protein targets and 6000 ligands. *Nucleic Acids Res.* **2016**, *44*, D1054−D1068.
(68) Mysinger, M. M.; Carchia, M.; Irwin, J. J.; Shoichet, B. K. Directory of useful decoys, enhanced (DUD-E): better ligands and decoys for better benchmarking. *J. Med. Chem.* **2012**, *55*, 6582−6594.
(69) Case, D. A.; Berryman, J. T.; Betz, R. M.; Cerutti, D. S.; Cheatham, I. T. E.; Darden, T. A.; Duke, R. E.; Giese, T. J.; Gohlke, H.; Goetz, A. W.; Homeyer, N.; Izadi, S.; Janowski, P.; Kaus, J.; Kovalenko, A.; Lee, T. S.; LeGrand, S.; Li, P.; Luchko, T.; Luo, R.; Madej, B.; Merz, K. M.; Monard, G.; Needham, P.; Nguyen, H.; Nguyen, H. T.; Omelyan, I.; Onufriev, A.; Roe, D. R.; Roitberg, A. E.; Salomon-Ferrer, R.; Simmerling, C. L.; Smith, W.; Swails, J.; Walker, R. C.; Wang, J.; Wolf, R. M.; Wu, X.; York, D. M.; Kollman, P. A. *AMBER 2015*; Universityof California: San Francisco, 2015.
(70) Mysinger, M. M.; Shoichet, B. K. Rapid context-dependent ligand desolvation in molecular docking. *J. Chem. Inf. Model.* **2010**, *50*, 1561−1573.
(71) Wei, B. Q.; Baase, W. A.; Weaver, L. H.; Matthews, B. W.; Shoichet, B. K. A model binding site for testing scoring functions in molecular docking. *J. Mol. Biol.* **2002**, *322*, 339−355.
(72) Word, J. M.; Lovell, S. C.; Richardson, J. S.; Richardson, D. C. Asparagine and glutamine: using hydrogen atom contacts in the choice of side-chain amide orientation1. *J. Mol. Biol.* **1999**, *285*, 1735−1747.
(73) Gallagher, K.; Sharp, K. Electrostatic contributions to heat capacity changes of DNA-ligand binding. *Biophys. J.* **1998**, *75*, 769−776.
(74) Sharp, K. A. Polyelectrolyte electrostatics: Salt dependence, entropic, and enthalpic contributions to free energy in the nonlinear Poisson−Boltzmann model. *Biopolymers* **1995**, *36*, 227−243.
(75) Olsen, R. H. J.; DiBerto, J. F.; English, J. G.; Glaudin, A. M.; Krumm, B. E.; Slocum, S. T.; Che, T.; Gavin, A. C.; McCorvy, J. D.; Roth, B. L.; Strachan, R. T. TRUPATH, an open-source biosensor platform for interrogating the GPCR transducerome. *Nat. Chem. Biol.* **2020**, *16*, 841−849.
(76) Barnea, G.; Strapps, W.; Herrada, G.; Berman, Y.; Ong, J.; Kloss, B.; Axel, R.; Lee, K. J. The genetic design of signaling cascades

https://doi.org/10.1021/acs.jmedchem.1c02031
J. Med. Chem. 2022, 65, 4201−4217

to record receptor activation. *Proc. Natl. Acad. Sci. U.S.A.* **2008**, *105*, 64−69.
(77) Jordan, M.; Schallhorn, A.; Wurm, F. M. Transfecting mammalian cells: optimization of critical parameters affecting calcium-phosphate precipitate formation. *Nucleic Acids Res.* **1996**, *24*, 596−601.
(78) Longo, P. A.; Kavran, J. M.; Kim, M. S.; Leahy, D. J. Transient Mammalian Cell Transfection with Polyethylenimine (PEI). *Laboratory Methods in Enzymology: DNA*; Methods in Enzymology; Elsevier Inc., 2013; Vol. *529*, pp 227−240.
(79) Chaplan, S. R.; Bach, F. W.; Pogrel, J. W.; Chung, J. M.; Yaksh, T. L. Quantitative assessment of tactile allodynia in the rat paw. *J. Neurosci. Methods* **1994**, *53*, 55−63.
(80) Wercberger, R.; Braz, J. M.; Weinrich, J. A.; Basbaum, A. I. Pain and itch processing by subpopulations of molecularly diverse spinal and trigeminal projection neurons. *Proc. Natl. Acad. Sci. U.S.A.* **2021**, *118*, No. e2105732118.

https://doi.org/10.1021/acs.jmedchem.1c02031
J. Med. Chem. 2022, 65, 4201−4217